Sensitivity of peak flow to the change of rainfall temporal pattern due to warmer climate

Sherien Fadhel[1,2],*, Miguel Angel Rico-Ramirez[1], Dawei Han[1]

[1]Department of Civil Engineering, University of Bristol, Bristol, United Kingdom

[2]Department of Civil Engineering, University of Al-Mustansiriyah, Baghdad, Iraq
*Correspondence to: E-mail: sa12372@my.bristol.ac.uk; Tel: +44 (0)7443187340;

Abstract

The widely used design storms in urban drainage networks has different drawbacks. One of them is that the shape of the rainfall temporal pattern is fixed regardless of climate change. However, previous studies have shown that the temporal pattern may scale with temperature due to climate change, which consequently affects peak flow. Thus, in addition to the scaling of the rainfall volume, the scaling relationship for the rainfall temporal pattern with temperature needs to be investigated by deriving the scaling values for each fraction within storm events, which is lacking in many parts of the world including the UK. Therefore, this study analysed rainfall data from 28 gauges close to the study area with a 15-min resolution as well as the daily temperature data. It was found that, at warmer temperatures, the rainfall temporal pattern becomes less uniform, with more intensive peak rainfall during higher intensive times and weaker rainfall during less intensive times. This is the case for storms with and without seasonal separations. In addition, the scaling values for both the rainfall volume and the rainfall fractions (i.e. each segment of rainfall temporal pattern) for the summer season were found to be higher than the corresponding results for the winter season. Applying the derived scaling values for the temporal pattern of the summer season in a hydrodynamic sewer network model produced high percentage change of peak flow between the current and future climate. This study on the scaling of rainfall fractions is the first in the

UK, and its findings are of importance to modellers and designers of sewer systems because it can provide more robust scenarios for flooding mitigation in urban areas.

Keywords*: rainfall temporal pattern; scaling for rainfall volume and fraction; climate change; peak flow*

1. Introduction

The accurate design of urban drainage networks requires the continuous simulation of long rainfall time series using an urban drainage model, which results in long computational times, and later the results need to be statistically post-processed (Willems 2013; Butler & Davies 2011). To overcome this problem, a design rainfall hyetograph with a specific temporal pattern, which is known as a design storm, is used instead in practice (Yen & Chow 1980; Wenzel 1982; Willems 2000; Madsen et al. 2002). Design storms can be derived by following one of two distinct approaches. The first approach is to extract the rainfall intensity from intensity–duration–frequency (IDF) curves and apply an arbitrary temporal distribution to that intensity to obtain the design storm (Keifer & Chu 1957; Desbordes 1978). The second approach is to analyse specific storm events from the observed rainfall data to derive the temporal distribution (Huff 1967; Nguyen et al. 2010). For both approaches a statistical analysis is performed before the hydrological model simulations. The statistical analysis has assumed that the frequency of urban drainage peak flow is equal to the corresponding frequency of the rainfall event. Such assumption is applied for areas that have a large proportion of paving, which is most often the case for urban runoff. Also, when the concentration time is almost constant for a specific location in the drainage system. In addition, such areas should have no strong seasonal variation such as watershed hydrology

where the soil saturation level can affect the runoff. For the above conditions, the high rainfall intensities at a given location result in large peak sewer flows.

Different design storms have been derived, developed, and adopted around the world. Keifer and Chu (1957) were the first to develop the Chicago storm in the USA, and later other alternative patterns were developed; for example, by Silfada (1973), Pilgrim and Cordery (1975), the UK *Flood Studies Report* (FSR 1975), Desbordes (1978), Yen and Chow (1980), and the UK *Flood Estimation Handbook* (FEH 1999). The drawbacks of these approaches have been summarised in many previous studies (McPherson 1978; Walesh 1979; James & Robinson 1982; Rivard 1996). One of the shortcomings of these approaches that this study seeks to address concerns the fixing of the shape of the temporal pattern for rainfall storms regardless of changes in the climate. Using the current approaches, a specific current rainfall intensity is expected to appear in the future but with a shorter return period (IPCC 2012). If we apply the temporal pattern of any of the abovementioned design storms for this rainfall intensity and for two different climates (i.e. current and future climates), the two storms will end up with exactly the same temporal distribution and peaks at the same location. However, Wasko and Sharma (2015) showed that the rainfall temporal pattern in Australia is changing with temperature due to climate change. The observed relation between rainfall and temperature, which is known as scaling, results from the natural variability in the present climate. The authors investigated the scaling values for each fraction of the rainfall temporal pattern and have found that the highest rainfall fraction scales positively, while the lowest fraction scales negatively with temperature regardless of the season and the type of event (see Figure1 in Wasko & Sharma 2015). The adjustment of the temporal pattern for a range of temperature changes using different scaling values for different locations (depending on the location of the station where the scaling is derived) was found to greatly affect the peak flood value in these locations (Wasko & Sharma 2015). Another recent study by Muller & et al.

74 2017 confirms the findings of Wasko & Sharma 2015 in which changing the shape of rainfall
75 event has a great effect on the peak flow of combined sewer system. However, the authors in
76 Muller & et al. 2017 study adopt a continuous rainfall time series instead of design storms.

77 For the UK climate, all the previous studies have investigated the scaling relationship
78 concentrated on the scaling of the overall storm event intensity, termed as storm volume, and
79 the most recent of these studies have investigated such a relation for sub-daily data, and more
80 specifically for extreme hourly data (Jones et al. 2014; Blenkinsop et al. 2015; Chan et al.
81 2016). However, none of the previous studies examined the scaling values for the UK climate
82 for the individual fractions of storm event (i.e. rainfall temporal pattern) (see section 3.1 for
83 the definitions and more details of rainfall volume and rainfall fractions). It would be of
84 interest to the hydrological community to explore such an issue besides Australia so that a
85 more complete pattern around the world could be derived.

86 Thus, the objectives of this study are to: (1) study the scaling relationship for both the storm
87 volume and the individual fractions of the storm event, termed the temporal pattern; for
88 storms with and without seasonal separation and (2) investigate how a change in the temporal
89 pattern can affect the peak flow of the sewer system of a particular urban area for the future
90 climate.

91

92 **2. Catchment and observed data**

93 The study area, which is a small urban catchment with an area of approximately 12 km x 5
94 km, is located in West Yorkshire in the north of England. The UK Environment Agency (EA)
95 provides rainfall data at a 15-min temporal resolution from tipping bucket gauges that cover
96 large parts of the UK. However, all the gauges provided by the EA were located outside the
97 study area, thus only the 28 closest gauges were used for this study (Figure 1). As shown in

Figure 1, some of the gauges are located far away from the catchment at distances of more than 40 km. Thus they may not seem relevant to the study area. However, these gauges were included in order to investigate whether there is a link between scaling values and altitude, as concluded by Wasko and Sharma (2015) for Australia, or not as found by Blenkinsop et al. (2015) for the UK. A quality check of the gauges was performed by using the procedure in Fadhel et al. (2016). The procedure consists of two steps: First, the spatial consistency between nearby gauges is tested (i.e. the gauge being tested is compared with neighbouring gauges). Second, the gauges that are flagged up as a result of the first check are subjected to another test using radar data. This is because rainfall is highly variable in space and time, so the performance of a gauge during a convective storm is not necessarily consistent spatially with that of neighbouring gauges. It should be noted that when the period of rainfall data for the gauges was not covered by the radar data (i.e. before 2006 in this study) only the first quality check was used. The temporal coverage for each gauge is shown in the table in Figure 1.

Figure 1. Study area and location of rain gauges. The number above each gauge (which is based on the distance of the gauge from the centre of the study area) is also used in the table that shows the temporal coverage for each gauge.

The daily temperature data used in this study was the gridded temperature data provided by the climate hydrology and ecology research support system meteorology dataset (CHESS-met) (1961–2015) and was at the 1-km space scale. The CHESS-met air temperature was derived by Robinson et al. (2015) for a reference height of 1.2 m. The authors interpolated the MORECS air temperature from a scale of 40 km to a 1-km resolution based on the bicubic spline method. Later, the integrated hydrological digital terrain model was adopted to adjust the elevation for each pixel of the 1-km grid interpolated data. The 1-km spatial resolution of temperature data may be too high for daily data and lower resolution data could

also (or better) be used. Further studies are needed based spatial correlation or semivariograms in order to work out the spatial variability of temperature distribution in the study area. A suitable spatial temperature resolution could then be derived.

The CHESS-met temperature data for the period 2004–2015 was used alongside the rainfall data to derive the scaling values.

3. Methodology

3.1 Scaling for rainfall volume and rainfall temporal pattern

The procedure in Wasko and Sharma (2015) was adopted to study the scaling relationship for both the storm volume (which is defined as the total rainfall depth in mm for a given storm event duration) and the storm fractions for five different durations. The largest 500 storm events in terms of volume for each rain gauge within the common period for all gauges (2004-2015) and a given duration were chosen (Wasko and Sharma 2015). Extracting such a high number of events ensures that all the heavy rainfall events that occur over the year are considered. Independent events were identified by using the criteria defined in Willems (2000), where two extreme events should be separated by at least a 12-h time interval if the duration is less than 12 h, while for longer durations a time interval larger than the considered duration should be used to delineate the independent events.

Various storm event durations, ranging from 1 h to 24 h, were included in the study (the values of the durations are shown in Figure 3). Since the gauge network used in this study has a 15-min resolution, the maximum number of fractions for a storm duration of 1 hour can only be four (i.e. each fraction has a timescale of 15 min). Thus, to be consistent with storms of other durations the fractions also need to be four in number as well. Therefore, for each

148 duration, the precipitation records were accumulated to ensure that the storm events were
149 grouped in exactly four periods in length. For example, to analyse a 3-h storm event, the
150 rainfall was accumulated into durations of 45 min to end up with a storm of four increments
151 of equal duration. Similarly, a 6-h storm event was split into four increments consisting of
152 four 90-min increments. Later, each storm event was matched to its concurrent temperature.

153 Most of the previous studies adopt the binning method to derive the scaling values for the
154 rainfall-temperature relationship. The method involves binning rainfall data in temperature
155 bins so that later the trend in the rainfall percentiles in each bin with temperature can be
156 investigated (Lenderink & van Meijgaard, 2008; Hardwick-Jones et al., 2010; Lenderink et
157 al., 2011). However, Wasko and Sharma (2014) showed that the binning method was
158 sensitive to the sample size, whereas quantile regression is unbiased towards the size. The
159 quantile regression derives the scaling of rainfall volume (α_v) with temperature by fitting an
160 exponential regression model to rainfall–temperature pairs, where the logarithm of rainfall
161 volume was regressed against temperature for the high percentile *q99* (Hardwick et al. 2010;
162 Wasko & Sharma 2014, 2015). Therefore, in this study, a quantile regression was performed
163 by using the R package, 'quantreq' (Koenker 2013) to find the scaling values for storms with
164 and without seasonal separation.

165 To construct the temporal patterns, the storm event was divided by its volume, then each
166 fraction within the pattern was ranked from the largest to the smallest. The scaling of the
167 ranked fractions with temperature was found by fitting the following equation (Wasko &
168 Sharma 2015):

169 $$P_{T+\Delta T}^{i} = P_{T}^{i}(1+\alpha_i)^{\Delta T} \quad \text{.....(1)}$$

170 where α_i is the rate at which the rainfall proportion for rank *i* of the temporal pattern changes
171 per degree of temperature; P_T^i is the *i*th rank rainfall fraction corresponding to temperature *T*;

and ΔT is the difference in Temperature. The statistical significance of the results at the 95% level was tested by using a t-test for the hypothesis that the slope of the regression line differs from zero against the null hypothesis that the slope is zero. In addition, the confidence intervals (i.e. uncertainty bound) of the scaling results were obtained under the same assumption. These confidence intervals are computed by the rank inversion method (Koenker, 2005).

It is worth noting that the length of the data used in this study was 12 years (i.e. the common period between the gauges), which is consistent with the temporal coverage investigated in previous studies that address the scaling relation (Hardwick et al. 2010; Wasko & Sharma 2014). However, one could argue that this data length is insufficient and may produce high uncertainty in the scaling results. Therefore, we investigated the effect of the temporal length on the scaling values (see section 4.2.3.2) to explore how the data length affects the uncertainty of the results.

3.2 Urban runoff model and hydrodynamic sewer flow model

The major parts of the sewer system in the study area carry both the urban rainfall runoff and the domestic and trade wastewater. The modelled sewer system was formed of 444 links, 432 nodes, 13 pumps, and 134 sub-catchments. The areas of sub-catchments ranged in size from 0.1 to 300 ha, and the total length of the sewer conduits was approximately 60 km. The total contributing area of the sub-catchments was 11.06 km^2, where 0.71 km^2 was classed as impermeable and 10.35 km^2 as pervious (Liguori et al. 2012; Rico-Ramirez et al. 2015). The study area was located in the Pennine Hills, thus the sewer system is relatively steep.

The rainfall-runoff process for the urban area in addition to the flow through the sewer network conduits was modelled by using a hydrodynamic sewer network model (Infoworks

196 CS) in order to study the sensitivity of the peak flow to the change in the rainfall temporal
197 pattern due to warmer climate. A combination of models for rainfall-runoff volume and
198 runoff routing for the different sub-catchments are available in the Infoworks CS model. For
199 example, the New UK Percentage Runoff model (Packman 1990) is used to find the runoff
200 volume for pervious areas, while the Wallingford model or the fixed runoff coefficient is
201 used for impermeable areas. The catchment runoff routing was found by using the Double
202 Linear Reservoir model (Sarginson & Nussey 1982). The Infoworks CS software calculates
203 the flow through the sewer conduits by solving the full St Venant equations.

204 The Infoworks CS sewer model was calibrated by following the current UK industrial
205 practice (WaPUG 2002). The range of rainfall depths and peak rainfall intensities for the
206 three events used for the model calibration were between 9.8 and 35 mm and 6.0 and 14.4
207 mm/h, respectively (Liguori et al. 2012; Rico-Ramirez et al. 2015). In 2007, seven depth
208 monitors and sixteen flow monitors were installed in the sewer system and upstream of most
209 of the pumping stations (Liguori et al. 2012). These monitors collected data at a frequency of
210 2 min. The locations of the flow monitors which are shown in the schematic plot of the
211 monitoring network in Figure 2, were adopted to address the sensitivity of peak flow to the
212 change of rainfall temporal pattern at each location. The main combined sewer overflow
213 structure that serves the centre of the study area is located just downstream of the flow
214 monitors FM015 and FM115 and upstream of FM017. In section 4.3, the results for flow
215 monitor FM015 are discussed in more detail due to the sensitive location of this flow
216 monitor; however, the results for other 15 flow monitors are also investigated.

217 Figure 2. Schematic overview of the monitoring network (Liguori et al. 2012).

218

219 ## 4. Results and discussion

4.1 Scaling values for all storms without seasonal separation

The scaling values for storm volumes and fractions were investigated for storms with and without seasonal separation. For the data without seasonal separation, Figure 3 shows the scaling of five different durations storm event volume (α_v) at each gauge. For hourly storm event volume where a statistically significant positive scaling for storm volume of 1.6% per °C to 4.88% per °C is shown by most of the gauges for the high percentile *q99* (Figure 3 top left).These results are consistent with Blenkinsop et al. (2015) in which there is no pattern that may refer to regional climatic controls on the scaling relationship between rainfall and temperature (i.e. there is no link between scaling values and altitude).

Figure 3. Rainfall scaling volume for all storms without seasonal separation. Each subplot is for a specific duration. Green circles correspond to positive scaling, while orange squares correspond to negative scaling. Crosses indicate statistical significance at the 95% confidence level.

Subsequently, each hourly storm event was divided into four periods, each having a duration of 15 min. For the largest rainfall fraction (α_1) and the high percentile *q99*, almost all the sites show a statistically significant positive scaling of approximately 0.8–3.3% per °C (Figure 4). In contrast, all the sites show a negative scaling for the smallest rainfall fraction (α_4) with a magnitude ranging from −0.06% to -1% per °C. However, the results are statistically significant for only a few sites. Also, the number of sites that show statistically significant results for the four fractions is higher for the first fraction, and decreases gradually to the last fraction (Figure 4). However, the negative scaling for the smallest rainfall fraction within the storm event means that such a fraction is scaling negatively even though the entire storm volume is scaling positively. In addition, the scaling values for the second fraction range between 0.8 to 2% per °C, while only the third fraction gives mixed results (i.e.

245 negatively and positively statistically significant scaling in the range of -0.8% to 0.9% per
246 °C).

247 Figure 4. Scaling for rainfall fractions for hourly storm event (storms without seasonal
248 separation). Green circles correspond to positive scaling, while orange squares correspond to
249 negative scaling. Crosses indicate statistical significance at the 95% confidence level.

250

251 An analysis of the results for the four fractions revealed a transition in the scaling values from
252 the largest to the smallest fraction, where the highest positive scaling with temperature is
253 shown by the first rank fraction, while the fourth rank fraction shows the highest negative
254 scaling with temperature. The intermediate fractions exhibit a declining scaling with
255 increasing rank. In Wasko and Sharma (2015), the temporal patterns of most of the sites
256 showed a peak-like structure, where, on average, the greatest magnitude occurs in the second
257 rainfall fraction (see Figure S4 in Wasko & Sharma 2015). However, the results of this study
258 reveal that the structure of the temporal pattern varies across the different durations and
259 according to whether the data are seasonally separated or not. For example, structure (A) in
260 Figure 5 is shown by most of the durations, especially the summer season (discussed in the
261 next section). The Table in Figure 5 shows the structure type of the temporal pattern for each
262 duration, and for storms with and without seasonal separation.

263 Figure 5. Derived structure types for the dominant rainfall temporal pattern depending on
264 rainfall duration and weather the data are seasonally separated or not. The index T correspond
265 to the length of rainfall duration.

266

267 The above analysis of scaling for rainfall volume and fractions was repeated for the other
268 four storm durations, and for each duration considered, the temporal pattern consisted of four
269 equal periods. For almost half of the sites the scaling of the volume decreases further as the
270 storm duration lengthens (Figure 3). The scaling for the rainfall fractions was found to be

271 consistent for all durations, in that the peak/weaker fraction becomes more/less intense at
272 higher temperatures, regardless the significance of the results over the durations. However,
273 from a comparison of the magnitude of scaling for each segment of the temporal pattern with
274 the corresponding segments for different durations, no obvious trends were observed. It is
275 worth noting that the scaling values for all rainfall fractions and the high percentile *q99* were
276 insignificant for all gauges and the last two durations. While for the second and third
277 durations, the number of the gauges that show significant results were consistent with that of
278 1 h duration in which it decreasing gradually from the first to the last fraction.

279 In addition, the range of uncertainty for the scaling results (i.e. both the scaling volume and
280 the rainfall fractions) was checked. For the scaling volume, the uncertainty bound for most of
281 the gauges is within the limit of -1.5 to 5. This is the case for all durations except the first
282 duration (i.e. 1 h), where the uncertainty limit is between -1 and 8 (Figure 6). However, only
283 a few gauges have an uncertainty range that is higher than the previous limits. Regarding the
284 uncertainty bound for the rainfall fractions, such range shows a transition in the limit values
285 between the fractions, which is consistent with the transition in the scaling values from the
286 largest to the smallest fraction. For example, Figure 7 shows that the uncertainty range for the
287 first fraction of the hourly storm duration is between -0.8 and 2.5 for most of the gauges. This
288 limit changes gradually from -1 and 2.5 and -1.8 and 0.8 for the second and third fractions,
289 respectively, while the range of uncertainty for the last fraction is between -1.8 and 0.5. Also,
290 the bound of uncertainty for the rainfall fractions is different for different storm durations.
291 However, the uncertainty results for rainfall fractions are consistent to those for the hourly
292 duration, in that the bound of uncertainty changes gradually across rainfall fractions (i.e. from
293 the first fraction to the fourth fraction).

294 Figure 6. Uncertainty bounds of the 95% significant level for rainfall scaling volume and all
295 storms without seasonal separation. Each subplot is for a specific duration.

Figure 7. Uncertainty bounds of the 95% significant level for rainfall fractions and hourly storm events (storms without seasonal separation). Each subplot is for a specific fraction.

4.2 Scaling values for storms with seasonal separation

Previous studies have shown that the season and the storm type can affect the rainfall–temperature scaling relationship due to the various temperature ranges examined and the nature of the various storm types that are predominant during the different seasons (Berg et al. 2009; Berg et al. 2013; Wasko & Sharma 2014, 2015). In this study, only a seasonal analysis was performed because Rico-Ramirez et al. (2015) showed that for the same UK study area, most of the convective storms fall within the summer season while stratiform storms occur during the winter season. In addition, the results of an analysis of the peaks over threshold events as well as the median annual maxima statistic reported in Blenkinsop et al. (2015) showed that extreme hourly convective events are most likely to occur in the summer season for most of the locations in the UK. Thus, no separate analysis of storm type is presented in this study.

For the UK, Blenkinsop et al. (2015) showed that the largest scaling value is seen in the summer season (6.9% per °C), while for the other seasons it is lower: 3.2% per °C for winter, 4.7% per °C for spring, and 3.9% per °C for autumn. From a comparison of the results in Blenkinsop et al. (2015) with the above results for the scaling of storms without seasonal separation, it is very clear that seasonal scaling in the UK is considerably different from the scaling value for storms without seasonal separation. In contrast, in Australia, Wasko and Sharma (2015) found that the scaling values for storms with and without seasonal separation

were almost the same. This is because in the northern half of Australia summer precipitation is dominant, while winter precipitation is dominant in the southern half of Australia.

4.2.1 Scaling values for summer season storms

In this study, the scaling values for both the storm volume and the fractions were found for the summer (JJA) and winter (DJF) seasons. Figure S.1 in the supplementary material shows the scaling value for summer rainfall volume and five durations. It is clear from the figure that the scaling value for the high percentile *q99* and hourly summer rainfall is consistent with Blenkinsop et al. (2015), where $\alpha_v \approx 9.2\%$ per °C for the middle of the UK (see Figure 3 in Blenkinsop et al. 2015). It is also clear from Figure S.1 that the scaling value for summer rainfall volume falls as the rainfall duration increases. Negative scaling values are shown by only a few stations from the second duration, such a number of stations with negative values increased gradually with duration increase to peak at the 12 h duration. However, some gauges show the opposite result, where the scaling starts to rise once again for the 24-h storm duration. This might have occurred because not all summer storms are convective; some are a mixture of convective and stratiform storms, which affects the signal of scaling (Berg & Haerter, 2011). Another explanation for this might be because of the short sample size which affects the scaling values. Such positive scaling values for 24hr duration must be excluded from the summer storms since it provides false results. However, we have kept it only to show the reader which gauges have untrusted results for a longer duration.

In addition, the scaling values for the 1-h duration and different percentiles (*q99*, *q90*, *q50*) are consistent with the results of Blenkinsop et al. (2015), where the scaling values for most of the gauges rise for the higher percentiles (Figure S.2 in the supplementary material). This is also the case for the two durations of 3 h and 6 h. However, for longer durations, the

345 scaling values vary; either rising or declining for the higher percentiles. As regards the
346 significance of the results for different percentiles, it was found that most of the gauges show
347 significant scaling results for rainfall volume for higher percentiles and especially for short
348 durations. For example, all the gauges show significant results except four and eight gauges
349 for the durations of 1-h and 3-h respectively.

350 An investigation of the scaling values for summer rainfall fractions revealed that the results
351 for all the durations and for the four fractions were insignificant for the high percentile *q99*
352 for all the stations, thus the calculation was repeated for lower percentiles (*q90, q50)*. The
353 results show that the scaling values for the last two fractions are lower for lower percentiles
354 for most of the stations. However, for the first two fractions, the scaling values vary across
355 the stations, either rising or falling for lower percentiles. In addition, the significance of the
356 results increased for lower percentiles and all durations, which is opposite to the results for
357 the scaling volume.

358 Apart from the significance of the results, for all percentiles and each duration, the temporal
359 pattern shows the same structure as that described above for rainfall without seasonal
360 separation; it peaks in the first rank fraction, which has the largest positive scaling, while the
361 largest negative scaling appears in the fourth rank fraction. The intermediate fractions exhibit
362 a decline in scaling by increasing rank (Figure S.3 in the supplementary material).

363

364 **4.2.2 Scaling values for winter season storms**

365 The scaling values for rainfall volume and five durations were also analysed for the winter
366 season (Figure S.4 in the supplementary material). The results are interesting and completely
367 opposite to those for the summer season. The scaling values were lowest for the shorter
368 durations, but after the duration of 3 h (shown by most of the stations) the scaling value rose

gradually by duration increase, where the largest scaling value is shown mostly for the 24-h duration. This is because stratiform storms dominant winter season storms. As in Blenkinsop et al. (2015), the scaling value for the winter hourly rainfall volume is higher for lower percentiles, which also the same for the duration of 3 h. While for longer durations most of the gauges show lower scaling values for lower percentiles. It is worth noting that the number of gauges which show significant scaling results for rainfall volume is higher for the winter season than for the summer season for all durations and all percentiles. In contrast, the number of gauges that show significant results for the scaling fractions for the winter season is lower than that for the summer season for all durations and specifically the percentile *q90*. Table S.1 summarizes the number of gauges showing positive and negative scaling values for all durations, percentiles, and storms (i.e. storms with and without seasonal separation) regardless of the significance of the results.

Again, the temporal pattern for the winter season has a structure that peaks at the first rank fraction, while the lowest value is found at the fourth rank fraction and scaling values for the other two fractions are of declining values.

The scaling values for the rainfall volume and the two seasons summer and winter are consistent with the corresponding results for the scaling of storms without seasonal separation in which no trend was obvious with respect to a regional climatic control (i.e. altitude) influencing the scaling value. In addition, no trends were observed for the two seasons from a comparison of the scaling value for each segment of the temporal pattern with those segments for different durations, which is similar to the results presented in section 4.1.

4.2.3 Uncertainty of scaling values for seasonal storms

As mentioned earlier, the scaling results for all storms (i.e. with and without seasonal separation), all durations, and different percentiles were within the 95% confidence interval. A sample of the results is shown in Figure 6. However, for some gauges the confidence interval of the scaling values is wide, reflecting the high uncertainty in the results for those gauges. This uncertainty may have been caused by the temporal length of the gauges (i.e. 12 years) adopted for the study, or by the number of storms used to derive the scaling values (i.e. 500). Therefore we tested the effect of these two sources of uncertainty on the scaling results, as discussed below.

4.2.3.1 Uncertainty of scaling values resulted from number of storms

The scaling values for rainfall volume were tested against the number of storms used for deriving the scaling values. Thus, the largest 200 storm events were used instead of 500 in order to determine whether the number of storms affects the scaling value and the significance of the results (Wasko & Sharma 2015). For the largest 200 storm events, all the gauges showed lower scaling values and insignificant results compared to the corresponding results for the 500 storm events for all durations, the two seasons summer and winter, and the high percentile *q99*. Therefore, the largest 200 storm events were tested again for the percentile *q90*, and the results for the summer season showed that the scaling value for the rainfall volume rose compared to the corresponding results for 500 storm events (Figure S.5 in the supplementary material). This was the case for all the durations, except for the last one where the reverse occurred. However, for the winter season, reducing the number of storms resulted in increased scaling values for the first two durations, while the reverse occurred for the last two durations and the results for the third duration were almost equally divided between the number of gauges that showed higher and those that showed lower scaling values

(Figure S.6 in the supplementary material). In addition, the uncertainty bound for the largest 200 storm events and the two seasons, summer and winter are computed and compared with the corresponding results for the uncertainty bound for the largest 500 storm events. It is clear from Figures 8 and S.7 that, in general, most of the gauges show small differences between the two uncertainty bounds for the two cases of storm events (i.e. 200 and 500). This is the case for all durations and the two seasons, summer and winter. However, in some cases, when there is a difference between the two bounds of uncertainty, this is due to the high range that is shown by the case of 200 storm events (e.g. Figure S.7, 1-h duration, gauges 4 to 10). It is worth noting that the effect of the uncertainty bound from the two cases of number of storm events on the peak flow of the sewer system has been addressed in section 4.3.

Figure 8. Uncertainty bounds of the 95% significant level for summer rainfall scaling volume due to the effect of number of storms (i.e. largest 500 and 200 storm bursts). Each subplot is for a specific duration and the percentile *q90*.

4.2.3.2 Uncertainty of scaling values resulted from temporal length of data

The scaling values for rainfall volume were tested against the length of the data that was used to derive such values to investigate the uncertainty that may results from the temporal coverage of gauges. It is clear from the table in Figure 1 that the gauges can be divided into three groups based on their temporal coverage, with almost one third of the total number of gauges falling into each group. Thus, the scaling values of rainfall volume for summer and winter storms calculated again based on the total length of the time series data covered by the gauges and compared to the above derived scaling volume based on the common period for all gauges, which was 12 years (2004–2015). In order to make it easier to visualise how the scaling volume can change based on the length of the data, the differences in the scaling volume based on different temporal coverage from the corresponding values based on the 12 common years are calculated and sample of the results presented in Figure 9 for the summer

442 storms. It is clear from Figure 8 that the length of datasets have a considerable effect on the
443 derived scaling values because for each duration more than one third of the total number of
444 gauges shows higher differences in the scaling volume. The derived scaling volume based on
445 the most recent and common period for all gauges shows higher values compared to that
446 based on different temporal coverage. This is the case for most of the gauges which shows
447 differences in the scaling results within the durations of 1h, 6h and 24 h (green circles in
448 Figure 9), while the reverse occurred for the durations of 3h and 12 h (orange squares in
449 Figure 9). The effect of the data temporal length on the derived scaling volume for winter
450 storms are consistent with the above results for summer storms in which there is no period
451 that produces the highest scaling volume for all durations (Figure S.8 in the supplementary
452 material). It is clear from the above results that it is not essential that the most extreme
453 rainfall values occur within the most recent period. In other words, it is not essential that the
454 most recent period is warmer than the previous periods or that it produces the most intense
455 and extreme rainfall events, as confirmed by Fadhel et al (2017). Consequently, the length of
456 data can be considered as an important source of uncertainty that may affect the scaling
457 results. However, it should be noted that while the results of this study are based on only 12
458 years of data, they are still of value (especially as this study is the first of its kind conducted
459 in the UK) and can give an indication about the future changes in rainfall extremes in the UK
460 and how they may affect the flooding of sewer systems.

461 A further analysis of the effect of the length of data (i.e. gauges with different and same
462 temporal coverage) on the scaling results for rainfall fractions revealed that the differences in
463 the results for the gauges with different temporal coverage were much less noticeable than the
464 corresponding differences for scaling volume.

465 Figure 9. Differences in scaling volume based on the length of data for the summer season
466 and the percentile *q90*. Each subplot is for a specific duration. Green circles correspond to

higher scaling values derived based on the common period, while orange squares correspond to higher scaling values derived based on different temporal coverage.

Finally, by comparing the results of the UK and Australia, it is found that the scaling values of rainfall volume and first and last rainfall fractions for the summer season for the UK are larger than the corresponding results for Australia. This is the case when extracting storms based on the largest 500 and 200 storm events. However, the opposite behaviour is observed for the winter season storms. To explain this, previous studies show that the scaling relationship can be decomposed into thermodynamic and dynamic contributions (Emori & Brown 2005; Chen et al, 2011). Pfahl et al (2017) show that regional differences in extreme rainfall and scaling values around the globe are mainly due to the dynamic contribution (see Figure 3 in Pfahl et al (2017)). The effect of this dynamic contribution is related to the change in the vertical pressure velocity, the direct radiative response to the increase of CO_2, and other factors (see Pfahl et al (2017) for more details). This effect may therefore explain the difference between the scaling results for the UK in this study and those for Australia in Wasko & Sharma 2015.

4.3 Impact of rainfall temporal pattern scaling on the sewer system

The peak flow magnitude of a flood is significantly affected by changes in the rainfall pattern over time (Ball 1994; Singh & Woolhiser 2002). Generally, a more devastating flood peak is caused by less uniform storm events that lead to a greater return interval. In this study, the effect of the temporal pattern of rainfall on the percentage relative change between the peak flow of the current climate and that of the future climate and on the number of flooded nodes due to the temperature rise from climate change was investigated by using the Infoworks CS model.

492 Previous derived design storms in the UK showed that the 50% summer profile is appropriate
493 for urban areas, while the 75% winter profile is better for rural areas (FSR 1975; FEH 1999).
494 The 50% summer profile is peakier than the 75% winter profile and, consequently, the former
495 produces a higher peak flow and higher possibility of flooding. In addition, the scaling values
496 for the summer season derived in section 4.2.1 are higher than the corresponding results for
497 the winter season in section 4.2.2. Thus, the derived scaling and temporal pattern for the
498 summer season were adopted for this part of the study.

499 The temporal patterns for 1-h and 3-h durations were built by using the average scaling
500 results from the nearest three gauges to the study area to overcome the problems of varied
501 scaling and the varied significant results that were shown by the nearest gauges. The rainfall
502 values for the current and future climates for the above two durations were extracted from the
503 IDF curves that were recently derived for the study area by Fadhel et al. (2017) and for each
504 of the six return periods (the values of the return periods are shown in Table 1). Fadhel et al.
505 (2017) derived eight cases of IDF curves based on eight reference periods, which were used
506 to bias correct the modelled rainfall data in order to overcome the uncertainty that results
507 from the constant bias assumption during the bias correction based on one reference period.
508 Thus, for the future climate, the rainfall values for the mean and maximum climate ensemble
509 members over the eight reference periods were used in the analysis of this study. The
510 percentage change in the peak flow between the current and future climates as well as the
511 number of flooded nodes were explored by adopting two different approaches.

512 In the first approach, it was assumed that the same current rainfall intensity would appear in
513 the future (i.e. no scaling for the rainfall volume was applied), thus, only the temporal pattern
514 underwent scaling using a temperature range from 1°C to 5°C. Also, in this approach, the
515 rainfall intensity was disaggregated into finer time steps by applying the derived temporal
516 pattern of each of the two structures, A and B (Figure 5), in order to determine the extent to

517 which the type of temporal pattern affects the change in peak flow between the current and
518 future climate. In cases where the temporal pattern did not add to unity after scaling, it was
519 scaled to ensure that the rainfall volume did not change across the range of temperature rises
520 (Wasko and Sharma 2015). In the second approach, both the rainfall volume and the rainfall
521 fractions for the current climate were scaled with the above range of temperatures, and only
522 the temporal pattern of structure A was applied. In cases where the rainfall volume after
523 scaling for a temperature increase of 5°C was less than the extracted value of the maximum
524 climate ensemble member from the IDF curves in Fadhel et al. (2017), the temporal pattern
525 was applied for such an extracted value. However, if the scaled rainfall volume for a specific
526 temperature was higher than the maximum climate ensemble member, then the rainfall
527 volume for that temperature and the other higher temperature values were not taken into
528 account in the analysis.

529 For the two approaches, the six return periods for the extracted rainfall intensities from the
530 IDF curves were assumed to be the same as the return periods for the peak flow (Butler &
531 Davies 2011; Willems et al. 2013). Table 1 shows an example of the percentage increase in
532 peak flow for the flow monitor FM015; the two approached of rainfall temporal scaling; six
533 return periods; and the duration of 1h. While Table 2 shows sample of the results of the
534 percentage increase in peak flow for four flow monitors; the two approached of rainfall
535 temporal scaling; the return period of 2 years; and the two durations 1h and 3 h.

536

537 **4.3.1 Impact of rainfall temporal pattern scaling on sewer peak flow**

538 As a result of scaling only the temporal pattern, the derived pattern of type A and flow
539 monitor FM015 shows that for a 1-h rainfall duration and each return period, the percentage
540 of peak flow keeps increasing as the temperature rises (Table 1). However, for a specific

541 temperature value there was no particular trend for the percentage increase in peak flow as
542 the return period increases. For example, increasing the temperature from 1°C to 5°C results
543 in the highest percentage increase in peak flow for the 2-year return period, where the peak
544 flow rises from 1.31% per 1°C to 6.28% per 5°C. On the other hand, the lowest percentage
545 increase occurs in the case of two return periods, 50 years (for the temperature values 2°C
546 and 4°C) and 100 years (for the temperature values 1°C, 3°C, and 5°C), where the peak flow
547 rises from 0.44% per 1°C to 3.68% per 5°C.

548 From a comparison of the above results with those for the derived temporal pattern of type B,
549 it is clear that the pattern of type A produces a higher percentage increase in peak flow than
550 that of type B for the last three return periods and the temperature rise from 1°C to 5°C
551 (Table 1). On the other hand, type B shows the largest values for the percentage change in
552 peak flow between the current and future climates for the second return period. The highest
553 percentage of peak flow for the first and third return periods varies between the two types of
554 temporal pattern for a range of temperature rises. However, as regards the difference in the
555 magnitude of the percentage increase in peak flow between the two temporal patterns, it is
556 clear from the table that in some cases the two patterns show close results but with some
557 differences (e.g. the first return period), while in other cases the difference is high, at almost
558 double (e.g. the last three return periods and especially the last three temperature values). In
559 addition, Figure S.9 shows the flow-duration-frequency (FDF) graph for flow monitor
560 FM015 produced by scaling only the temporal pattern for the temperature range 1°C to 5 °C,
561 six return periods, and the two temporal patterns of structures A and B.

562

563 Table 1. Percentage of change of peak flow between the current and future climates for flow
564 monitor FM015 and the duration of 1h due to increase in temperature.

565 The sensitivity of the relative change in peak flow to future temperature change was also
566 tested by scaling both the rainfall volume and the rainfall fractions (by applying the temporal
567 pattern of type A) for a temperature rise from 1°C to 5°C. The results for flow monitor
568 FM015 show that the change in peak flow between the current and future climates for a 1-h
569 rainfall duration after scaling the rainfall volume and fractions is much greater than the
570 corresponding results produced by scaling the temporal pattern alone (Table 1). For example,
571 for a 5-year return period the peak flow increases from 10.85% per 1°C to 60.50% per 5°C
572 compared to 1.13% per 1°C to 5.79% per 5°C by scaling only the temporal pattern of type A.
573 It is worth noting that when scaling rainfall volume and fractions the percentage increase in
574 the peak flow declines as the return period increases for a specific temperature. However, it
575 increases as the temperature rises for a specific return period.
576 The above analysis was repeated for the 3-h duration and all six return periods. For this
577 duration and for flow monitor FM015, by scaling the temporal pattern only, the pattern of
578 type B shows a higher percentage increase in the peak flow between the current and future
579 climates than type A for all six return periods (the results not shown). On the other hand,
580 scaling both the rainfall volume and the rainfall fractions produces a change in the peak flow
581 for the 3-h duration that is similar to that for the 1-h duration, i.e. the percentage increase in
582 the peak flow is higher than when scaling only the rainfall fractions. However, the percentage
583 change in the peak flow between the current and future climates for the 3-h duration and flow
584 monitor FM015 are much lower than the corresponding results for the 1-h duration (Table 2
585 for FM015). In addition, for a specific temperature, applying both of the approaches to
586 scaling to the 3-h duration leads to almost constant results for the percentage change in the
587 peak flow over the return periods. For example, by scaling both the rainfall volume and
588 fractions for a 5°C increase in temperature, the percentage of increase for peak flow was
589 around 21% for the six return periods. It is worth noting that for the 3-h duration and each

590 return period, none of the scaled rainfall volumes for the temperature rise of 5°C are close to
591 those of the corresponding rainfall intensity of the maximum climate ensemble member.
592 Thus, the temporal pattern applied for the future rainfall intensity and each return period, and
593 the results for the percentage change in peak flow shown in Table 2 are the highest values
594 over the temperature range for each return period. In addition, the FDF graph for flow
595 monitor FM015 by scaling both rainfall volume and rainfall fractions is shown in Figure S.10
596 for the temperature range 1°C to 5 °C, six return periods, and the temporal pattern of
597 structure A.

598 The above analysis of flow monitor FM015 was repeated for the other 15 flow monitors and
599 Table 2 shows sample of the results for four flow monitors. The results for most of the flow
600 monitors are consistent, where for each return period the size of the peak flow for the future
601 climate increases as the temporal pattern of the rainfall changes due to the rise in temperature.
602 The percentage increase is higher when both the rainfall volume and the temporal pattern are
603 scaled. However, no obvious trend was observed by all flow monitors regarding the
604 maximum increase in the percentage change of peak flow with the return periods for a
605 specific rise in temperature. When only the temporal pattern is scaled, the results for the two
606 types of patterns with different structures show that for each duration neither pattern can
607 produce the maximum percentage increase in peak flow for all temperature ranges; all return
608 periods; and all flow monitors. It is worth noting that for some flow monitors, the percentage
609 change in the peak flow between the current and future climates is much higher than for
610 others, and this seems to depend on the sub-catchment area that drains to the flow monitor.

611 Table 2. Percentage of change of peak flow between the current and future climates for return
612 period of 2 years due to increase in temperature.

613 Finally the uncertainty range for the percentage of peak flow was checked by scaling both the
614 rainfall volume and rainfall fraction for all flow monitors. For this analysis we only adopt the
615 temporal pattern of structure A and the temperature range 1°C to 5°C and for the two cases of
616 storm numbers (i.e. largest 500 & 200 storm events). Figure S.11 shows the sample of the
617 results for the flow monitor FM015 and 1-h duration. It is clear from the figure that for each
618 return period the uncertainty bound for the percentage change of peak flow increases for
619 higher temperatures. Also, when comparing the uncertainty bound for all return periods and a
620 specific temperature, such uncertainty increases for longer return periods. This is the case
621 when testing the uncertainty bound for both the largest 500 & 200 storm events. In addition,
622 there is a small difference between the two uncertainty bounds for the two cases of storm
623 numbers.

624

625

626

627 **4.3.2 Impact of rainfall temporal pattern scaling on flooded nodes**

628 As a result of scaling the rainfall fractions on the number of flooded nodes, the two derived
629 patterns A and B show almost the same results for the number of flooded nodes for each
630 return period over the range of temperature increases. Table 3 shows the sample of the results
631 of the flooded nodes for the two approached of rainfall temporal scaling; six return periods;
632 and the duration of 1h. For the two durations of 1 h and 3 h, the number of flooded nodes
633 increases as the return period increases. However, the occurrence of dangerous flooding is
634 not indicated by the two temporal patterns for the first two return periods and for the whole
635 range of temperature increases. In addition, for the two durations and a specific return period,
636 as the temperature increases, the number of flooded nodes increases (e.g. return period of 10

637 years and pattern of type A; Table 3). For other return periods, the number of flooded nodes
638 remains constant either for the whole or part of the range of temperature increases (e.g. return
639 periods of 50 and 100 years and pattern of type B; Table 3). However, the largest number of
640 flooded nodes is seen for the largest return period and a 1-h duration with a range of 30 to33
641 nodes flooded over the temperature increase.

642 Table 3. Number of flooded nodes for 1 h duration due to climate change

643 The number of flooded nodes by scaling both the rainfall volume and rainfall fractions for the
644 temporal pattern of type A are higher than the corresponding results by scaling the rainfall
645 fractions alone (Table 3). However the results are similar to that by scaling the rainfall
646 fractions alone, where the number of flooded nodes increases with a rise in temperature for a
647 specific return period or with an increase in the return period for a specific temperature
648 (Table 3). In addition, the largest number of flooded nodes occurs for the 1-h duration,
649 compared to the results for the 3-h duration, and especially for the last return period (100
650 years) where the flooded nodes increase from 38 nodes for a 1°C increase to 63 nodes for a
651 5°C increase in temperature.

652 The uncertainty bound for the number of flooded nodes was checked by scaling the rainfall
653 volume and rainfall fractions for the temporal pattern of type A. The results are shown in
654 Figure S.12 and for the two cases of the number of storms (i.e. largest 500 & 200 storm
655 events). The uncertainty bounds in Figure S.12 increases as the temperature rises for a
656 specific return and as the return period increases for a specific temperature. This is the case
657 for the largest 500 & 200 storm events. In addition, the uncertainty bound for the two cases of
658 the number of storms shows only a small difference.

659

660 ## 5. Conclusions

Due to the lack of long-term flow data, design storms are still widely used in engineering practice to simulate design floods in sewer systems and to analyse the flood risk. One of the drawbacks of such storms is the fixing of the shape of the temporal profile of rainfall. However, previous studies showed that due to climate change each fraction of the rainfall profile scales with temperature in a different way. In other words, peak fractions become peakier and non-peak fractions become less so with the temperature rise due to climate change. Consequently, such changes in the storm profile may affect the peak flow of the drainage system and produce flooding. Thus, the sensitivity of peak flow to the changes in the temporal pattern of rainfall has been investigated by examining the scaling relationship between rainfall and temperature using the nearest 28 gauges to the study area.

The scaling values for the rainfall volume and the rainfall fractions were calculated with and without seasonal separation. It was found that the scaling results for rainfall volume without seasonal separation were very different from the corresponding results for rainfall volume with seasonal separation for all durations. Specifically, the largest scaling values were seen for hourly summer storms, and such values declined as the duration increased up to a certain limit (12 h) and then scaling increased again for the last duration; however, this value was still lower than those for shorter durations. The opposite behaviour was observed for the winter season, where the scaling values were found to be the lowest for short durations (1 h, 3 h) and got bigger with increasing duration, where the largest value was mostly commensurate with the longest duration (24 h). For all the data with and without seasonal separation, there was no trend for the regional climatic controls on the scaling value.

From an examination of the scaling values of temporal patterns within individual storm events, it was found that there was a consistent positive scaling for the largest rainfall fraction and a consistent negative scaling for the smallest rainfall fraction. This was the case for storms with and without seasonal separation, but there were also clear differences in the

686 fraction scaling values between storm types. In addition, it was observed that the results for
687 fraction scaling were insignificant for the high percentile *q99*. This was the case for the last
688 two durations and storms without seasonal separation, and for all durations for seasonally
689 separated storms. As for lower percentiles (*q90, q50*), the number of stations that showed
690 significant results increased for all durations, all fractions, and storms for the two seasons
691 summer and winter.

692 The derived temporal pattern for the summer season was applied to a hydrodynamic sewer
693 model in order to study the sensitivity of the peak flow to changes in the rainfall pattern due
694 to climate change. To this end, two different approaches were adopted. First, the rainfall
695 volume was fixed and the temporal pattern alone was scaled by applying and comparing two
696 of the derived patterns for the summer season. Second, both the rainfall volume and the
697 rainfall fractions were scaled with temperature change for only one pattern. The percentage
698 increase in the peak flow of 16 flow monitors as a result of scaling both the rainfall volume
699 and fractions was found to be much greater than the corresponding results caused by scaling
700 only the temporal pattern. This was the case for the two durations (1 h, 3 h); all return
701 periods; and all temperature values. However, there was no specific temporal pattern that
702 could show the maximum growth in the change of future peak flow for all return periods and
703 the two durations when scaling the temporal pattern alone.

704 In addition, the number of flooded nodes by scaling both the rainfall volume and the rainfall
705 fractions were higher than the corresponding results by scaling the rainfall fractions alone.
706 The largest number of flooded nodes were shown for the shorter durations, larger return
707 periods, and the highest increase of temperature.

708 Changes in peak flow due to climate change may result in serious consequences for sewer
709 systems and thus this aspect should be considered in the decision-making process for

designing new systems or upgrading the existing systems. The worst case scenario should be addressed carefully; even though it may not be used in the actual sewer system design, it can still give an indication as to how to mitigate sewer flooding through the adoption of flexible and sustainable solutions (Willems et al. 2012; Willems 2013; Fadhel et al. 2017).

Further research is required to examine some as yet untackled questions. For example, what results will be produced if the scaling values for the rainfall fractions are derived from another network with finer resolution? (so the temporal pattern can be divided into more than four fractions). By classifying the rainfall into convective and stratiform storms, does the scaling results be similar to the corresponding results of storms based on seasonal separation? Also, how will those results affect the peak flow and how the uncertainty of peak flow will be compared with the uncertainty of scaling volume? Even more interestingly, how will the results vary for different study areas? It is hoped that this study will stimulate the community to explore such questions further.

Acknowledgments

The authors thank the Environment Agency (https://www.gov.uk/government/organisations/environment-agency), for providing the rain gauges dataset. We also thank the Centre of Ecology and Hydrology for providing the gridded temperature data through (CHESS-met) dataset. More details about the CHESS-met data are available from https://catalogue.ceh.ac.uk/documents/b745e7b1-626c-4ccc-ac27-56582e77b900. The authors would like to thank Yorkshire Water Service Ltd. for providing the rainfall data for the urban catchment, as well as the sewer flow data and Infoworks CS model of the sewer system.

References

Ball, J. E. 1994. The influence of storm temporal patterns on catchment response. Journal of Hydrology 158, 285–303. doi: https://doi.org/10.1016/0022-1694(94)90058-2

Berg, P., Haerter, J. O., Thejll, P., Piani, C., Hagemann, S., & Christensen, J. H. 2009. Seasonal characteristics of the relationship between daily precipitation intensity and

surface temperature. *Journal of Geophysical Research-Atmospheres*, *114*. doi: Artn D18102 10.1029/2009jd012008

Berg, P., Haerter, J.O. 2011. Unexpected increase in precipitation intensity with temperature — A result of mixing of precipitation types? Atmos. Res. doi:10.1016/j.atmosres.2011.05.012

Berg, P., Moseley, C. & Haerter, J. O. 2013. Strong increase in convective precipitation in response to higher temperatures. Nature Geosci. 6, 181–185. doi:10.1038/ngeo1731

Blenkinsop, S., Chan, S. C., Kendon, E. J., Roberts, N. M., & Fowler, H. J. 2015. Temperature influences on intense UK hourly precipitation and dependency on large-scale circulation. *Environmental Research Letters*, *10*(5). doi:Artn 05402110.1088/1748-9326/10/5/054021

Butler. D & Davies. J.w. 2011. Urban Drainage. 3rd edn, Spon Press, Taylor & Francis, 625p.

Centre for Ecology & Hydrology, 1999. The *Flood Estimation Handbook* (five volumes). Volume 3: Statistical procedures for flood frequency estimation. Wallingford, UK.

Chan, S. C., Kendon, E. J., Roberts, N. M., Fowler, H. J., & Blenkinsop, S. 2016. Downturn in scaling of UK extreme rainfall with temperature for future hottest days. *Nature Geoscience*, *9*, 24-28. doi:10.1038/ngeo2596

Desbordes, M. 1978. Urban runoff and design storm modelling, Proc. of the First International Conference on Urban Storm Drainage, U.K. Pentech Press, London, U.K., pp. 353-361.

Fadhel, S., Rico-Ramirez, M.A. & Han, D. 2016. Exploration of an adaptive merging scheme for optimal. *Journal of Hydroinformatics*. doi: 10.2166/hydro.2016.022

Fadhel, S., Rico-Ramirez, M.A. & Han, D. 2017. Uncertainty of Intensity-Duration-Frequency (IDF) curves due to varied climate baseline periods. *Journal of Hydrology*. doi: http://dx.doi.org/10.1016/j.jhydrol.2017.02.013

Hardwick Jones, R., Westra, S. & Sharma, A. 2010. Observed relationships between extreme sub-daily precipitation, surface temperature, and relative humidity. Geophys. Res. Lett. 37, L22805. doi: 10.1029/2010GL045081

Huff, F. A. 1967. Time distribution of rainfall in heavy storms. Water Resour. Res. 3(4):1007-1019. doi: 10.1029/WR003i004p01007

786 Intergovernmental Panel on Climate Change (IPCC), 2012. Managing the risks of extreme
787 events and disasters to advance climate change adaptation. In: Field, C.B., et al.
788 (Eds.)A Special Report of Working Groups I and II of the Intergovernmental Panel on
789 ClimatChange, Cambridge University Press, New York.

790 James, W. & M. Robinson, 1982. Continuous Models Essential for Detention Design.
791 Proceedings, Stormwater Detention Facilities, ASCE, Henniker, New Hampshire, pp:
792 163-175.

793 Jones M R, Blenkinsop S, Fowler H J & Kilsby C G. 2014. Objective classification of
794 extreme rainfall regions for the UK and updated estimates of trends in regional
795 extreme rainfall, Int. J. Climatol. 34 751–65. doi: 10.1002/joc.3720

796 Kiefer, C. J., & H. H. Chu. 1957. Synthetic storm pattern for drainage design. J. Hydraul.
797 Div., Proc. Am. Soc. Civil Engrs. 83: 13 32-1-13 3 2-25.

798 Koenker, R. 2005, Quantile Regression. Cambridge U. Press.

799 Koenker, R. 2013, quantreg: Quantile Regression. [Available at http://CRAN.R-
800 project.org/package5quantreg.]
801
802 Lenderink, G., & E. van Meijgaard. 2008. Increase in hourly precipitation extremes beyond
803 expectations from temperature changes, Nat. Geosci., 1(8), 511–514,
804 doi:10.1038/ngeo262.
811
812 Lenderink, G., H. Y. Mok, T. C. Lee, & G. J. van Oldenborgh. 2011. Scaling and trends of
813 hourly precipitation extremes in two different climate zones: Hong Kong and the
814 Netherlands, Hydrol. Earth Syst. Sci., 15(9), 3033–3041, doi:10.5194/hess-15-3033-
815 2011.
816
817 Liguori, S., Rico-Ramirez, M. A., Schellart, A. N. A. & Saul, A. J. 2012. Using
818 probabilistic radar rainfall nowcasts and NWP forecasts for flow prediction in urban
819 catchments. Atmospheric Research 103, 80–95. doi: 10.1016/j.atmosres.2011.05.004.
820
821 Madsen, H., Mikkelsen, P. S., Rosbjerg, D., & Harremoes, P. 2002. Regional estimation of
822 rainfall intensity-duration-frequency curves using generalized least squares regression
823 of partial duration series statistics. *Water Resources Research, 38*(11). doi:Artn 1239
824 10.1029/2001wr001125
825

826 McPherson, M.B., 1978. Urban Runoff Control Planning. EPA-600/9-78-035,
827 Environmental Protection Agency, Washington, DC.

828 Müller, T.,Schütze, M., & , Bárdossy, A. 2017. Temporal asymmetry in precipitation time
829 series and its influence on flow simulations in combined sewer systems. *Advances in*
830 *Water Resources*,107, 56-64. doi: http://dx.doi.org/10.1016/j.advwatres.2017.06.010.
831

832 NERC 1975. Flood Studies Report (five volumes). Natural Environment Research Council
833 London (Vol. II, Meteorological Studies)

834 Nguyen, V.-T.-V., Desramaut, N. & Nguyen, T. D. 2010. Optimal rainfall temporal
835 patterns for urban drainage design in the context of climate change. Water Science
836 and Technology 62 (5), 1170–1176. doi: 10.2166/wst.2010.295.
837
838 Packman, J., 1990. New Hydrology model. WaPUG Spring Meeting. http://
839 www.ciwem.org/groups/wapug/ Accessed May 2011.
840
841 Pilgrim, D. H., & Cordery, I. 1975. Rainfall Temporal Patterns for Design Floods. *Journal*
842 *of the Hydraulics Division-Asce*, *101*(Nhy1), 81-95.
843
844 Rico-Ramirez, M. A., Liguori, S., & Schellart, A. N. A. 2015. Quantifying radar-rainfall
845 uncertainties in urban drainage flow modelling. *Journal of Hydrology*, *528*, 17-28.
846 doi:10.1016/j.jhydrol.2015.05.057
847
848 Rivard, G. 1996. "Design Storm Events for Urban Drainage Based on Historical Rainfall
849 Data: a Conceptual Framework for a Logical Approach." Journal of Water
850 Management Modeling Rl91-12. doi: 10.14796/JWMM.Rl91-12.
851 Robinson, E. L., Blyth, E., Clark, D. B., Finch, J., & Rudd, A. C. 2015. Climate hydrology
852 and ecology research support system potential evapotranspiration dataset for Great
853 Britain (1961-2012) [CHESS-PE]. NERC Environmental Information Data
854 Centre https://doi.org/10.5285/d329f4d6-95ba-4134-b77a-a377e0755653;
855
856 Sarginson, E.J., & Nussey, B.B., 1982. The explicit computation of urban runoff. Urban
857 Drainage Systems: Proceedings of the First International Seminar, Southampton,
858 England. September 1982 ISBN 0273085964.
859
860 Sifalda V. 1973. Entwicklung eines Berechnungsregens fur die ¨ Bemessung von
861 Kanalnetzen. GWF-Wasser/Abwasser 114: 435–440
862 Singh, V. P. & Woolhiser, D. a. 2002. Mathematical Modeling of Watershed Hydrology.
863 Journal of Hydrologic Engineering 7, 270–292. doi:
864 http://dx.doi.org/10.1061/(ASCE)1084-0699(2002)7:4(270)
865 Walesh, S.G., 1979. Summary Seminar on the Design Storm Concept. Proceedings,
866 Stormwater Management Model (SWMM) Users Group meeting, EPA 600/9-79-026.
867 WaPUG, 2002. Code of practice for the hydraulic modelling of sewer systems.
868 http://www.ciwem.org/groups/wapug/ Accessed May 2011.
869
870 Wasko, C., & Sharma, A. 2014. Quantile regression for investigating scaling of extreme
871 precipitation with temperature. *Water Resources Research*, *50*(4), 3608-3614.
872 doi:10.1002/ 2013WR015194.
873
874 Wasko, C., & Sharma, A. 2015. Steeper temporal distribution of rain intensity at higher
875 temperatures within Australian storms. *Nature Geoscience*, *8*(7), 527-U166.
876 doi:10.1038/Ngeo2456
877

878 Wenzel H. G. 1982. Rainfall for urban stormwater design. In: Urban Storm Water
879 Hydrology. Water Resour. Mongor. Ser., 7, D.F. Kibler (ed.), American Geophysical
880 Union, Washington, DC, pp. 35-67.

881 Willems P. 2000. Compound intensity/duration/frequency-relationships of extreme
882 precipitation for two seasons and two storm types. *Journal of Hydrology*., 233, 189-
883 205. doi: http://doi.org/10.1016/S0022-1694(00)00233-X

884 Willems, P. 2013. Revision of urban drainage design rules after assessment of climate
885 change impacts on precipitation extremes at Uccle, Belgium. *Journal of Hydrology,*
886 *496*, 166-177. doi:10.1016/j.jhydrol.2013.05.037
887

888 Yen, B.C, & V.T. Chow. (1980). Design hyetographs for small drainage structures, J. Hyd.
889 Div., Am. Soc. Civ. Eng., vol. 106, no HY6, pp. 1055-1076.

890

Table 1. Percentage of change of peak flow between the current and future climates for flow monitor FM015 and the duration of 1h due to the increase in temperature.

	Scaling rainfall fractions only												Scaling rainfall volume and rainfall fractions					
	Temporal pattern of type B						Temporal pattern of type A						Temporal pattern of type A					
Temp Range °C	2 year	5 year	10 year	25 year	50 year	100 year	2 year	5 year	10 year	25 year	50 year	100 year	2 year	5 year	10 year	25 year	50 year	100 year
1	1.29	1.93	2.60	0.58	0.20	0.44	1.31	1.13	1.25	1.04	0.85	0.44	12.57	10.85	10.39	8.99	7.72	6.95
2	2.13	3.98	3.30	1.47	1.00	1.10	2.49	2.25	2.28	1.93	1.30	2.04	25.72	21.86	21.35	17.45	15.43	13.92
3	3.98	4.99	3.45	1.48	1.07	1.40	3.79	3.08	3.73	3.44	2.86	2.63	39.34	35.47	31.80	26.55	22.51	20.45
4	4.82	5.53	4.42	2.16	2.22	1.97	4.86	4.71	4.35	3.44	3.17	3.28	54.04	48.41	41.93	34.53	29.27	28.91
5	5.63	6.81	4.79	3.46	2.80	2.08	6.28	5.79	5.48	4.28	4.11	3.68	-	60.50	51.17	41.93	38.32	38.31
															61.10	**51.22**	**48.36**	**43.27**

Bold numbers mean the temporal pattern applied for rainfall value of the maximum climate ensemble member extracted from IDF curves , while '–' mean the scaled rainfall value at that temperature exceed the rainfall value of the maximum climate ensemble member extracted from IDF curves

Table 2. Percentage of change of peak flow between the current and future climates for return period of 2 years due to the increase in temperature.

		Scaling rainfall fractions only								Scaling rainfall volume and fractions			
		Temporal pattern of type B				Temporal pattern of type A				Temporal pattern of type A			
Duration	Temp Range °C	FM001	FM015	FM018	FM115	FM001	FM015	FM018	FM115	FM001	FM015	FM018	FM115
1 h	1	0.48	1.29	0.65	1.16	0.69	1.31	0.51	0.55	6.13	12.57	6.67	4.73
	2	0.78	2.13	1.23	1.46	1.35	2.49	1.08	1.27	10.00	25.72	15.12	8.23
	3	1.1	3.98	1.52	1.71	1.99	3.79	1.73	1.75	13.21	39.34	24.18	13.38
	4	1.38	4.82	2.13	2.24	2.59	4.86	2.30	2.35	15.77	54.04	33.75	19.53
	5	1.71	5.63	2.69	2.66	3.28	6.28	2.76	2.71	-	-	-	-
3 h	1	1.35	1.32	0.55	1.24	1.21	1.16	0.48	1.11	5.26	5.13	2.11	4.80
	2	2.66	2.6	1.08	2.44	2.40	2.31	0.96	2.19	10.63	10.47	4.21	9.82
	3	3.95	3.85	1.59	3.62	3.55	3.43	1.41	3.25	16.29	16.05	6.49	15.09
	4	5.21	5.07	2.09	4.77	4.67	4.53	1.86	4.28	21.76	21.86	8.86	20.60
	5	6.43	6.27	2.57	5.89	5.76	5.60	2.29	5.28	28.41	27.93	11.25	26.39
										57.11	**58.87**	**23.62**	**56.34**

Bold numbers mean the temporal pattern applied for rainfall value of the maximum climate ensemble member extracted from IDF curves , while '–' mean the scaled rainfall value at that temperature exceed the rainfall value of the maximum climate ensemble member extracted from IDF curves

	Scaling rainfall fractions only												Scaling rainfall volume and rainfall fractions					
	Temporal pattern of type B						Temporal pattern of type A						Temporal pattern of type A					
Temp Range °C	2 year	5 year	10 year	25 year	50 year	100 year	2 year	5 year	10 year	25 year	50 year	100 year	2 year	5 year	10 year	25 year	50 year	100 year
0	0	2	7	19	25	30	0	0	6	17	24	30	0	0	6	17	24	30
1	0	2	8	19	25	30	0	1	7	19	24	30	0	5	16	22	30	38
2	0	2	8	21	25	30	0	1	7	19	24	32	0	8	19	28	38	42
3	0	2	8	21	25	31	0	1	8	19	24	33	0	16	24	38	43	54
4	0	2	9	21	25	31	0	1	9	19	25	33	3	19	30	42	54	58
5	0	3	10	22	25	33	0	1	9	20	25	33	5	25	38	54	58	63

Table 3. Number of flooded nodes for 1 h duration due to climate change

Zero temperature value mean current climate

Table S.1 Summary of the number of gauges showing positive and negative scaling values

all storms		
duration	**N**	**P**
1	2	26
3	7	21
6	6	22
12	9	19
24	10	18

Largest 500 storms q99				
	Summer storms		Winter storms	
duration	**N**	**P**	**N**	**P**
1	0	28	15	13
3	4	24	16	12
6	10	18	11	17
12	19	9	6	22
24	14	14*	3	25

largest 500 storms q90				
	Summer storms		Winter storms	
duration	**N**	**P**	**N**	**P**
1	0	28	7	21
3	1	27	5	23
6	5	23	10	18
12	9	19	10	18
24	6	22	10	18

largest 500 storms q50				
	Summer storms		Winter storms	
duration	**N**	**P**	**N**	**P**
1	0	28	1	27
3	9	19	1	27
6	10	18	9	19
12	17	11	11	17
24	14	14*	13	15

largest 200 storms q90				
	Summer storms		Winter storms	
duration	**N**	**P**	**N**	**P**
1	0	28	12	16
3	1	27	14	14
6	6	22	12	16
12	7	21	10	18
24	8	20	6	12

N: negative values, P: positive values

Figure 1

Click here to download high resolution image

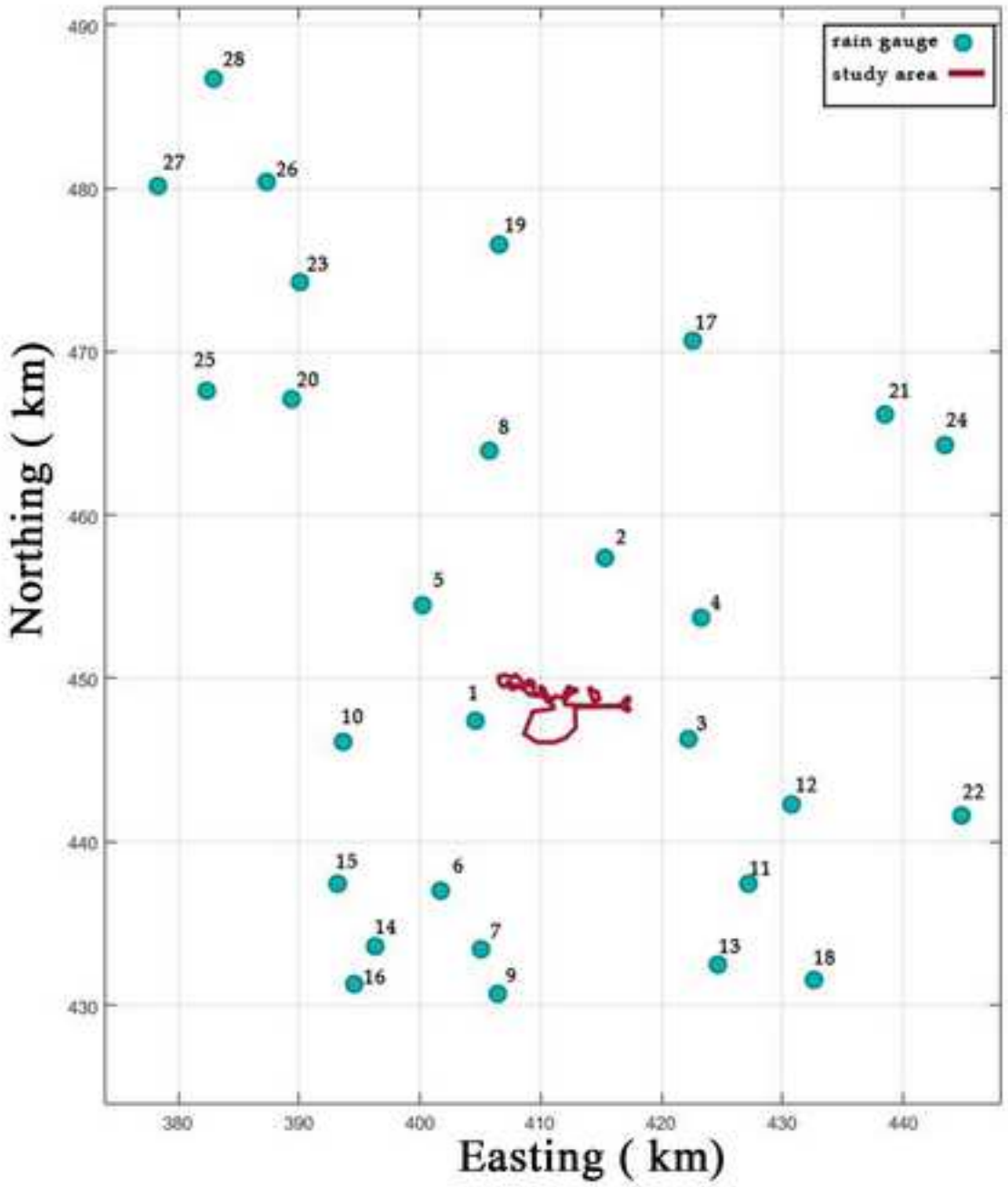

No.	From	To
1	2001	2016
2	2000	2016
3	1985	2015
4	1997	2015
5	1986	2016
6	2000	2016
7	2000	2016
8	2000	2016
9	2002	2016
10	2005	2016
11	1996	2016
12	1986	2016
13	1987	2016
14	2004	2016
15	1998	2016
16	1987	2016
17	1989	2015
18	1986	2016
19	1988	2015
20	1984	2014
21	2004	2015
22	1987	2016
23	2004	2015
24	1985	2015
25	1990	2016
26	2004	2015
27	1994	2016
28	1985	2015

Figure 2

Click here to download high resolution image

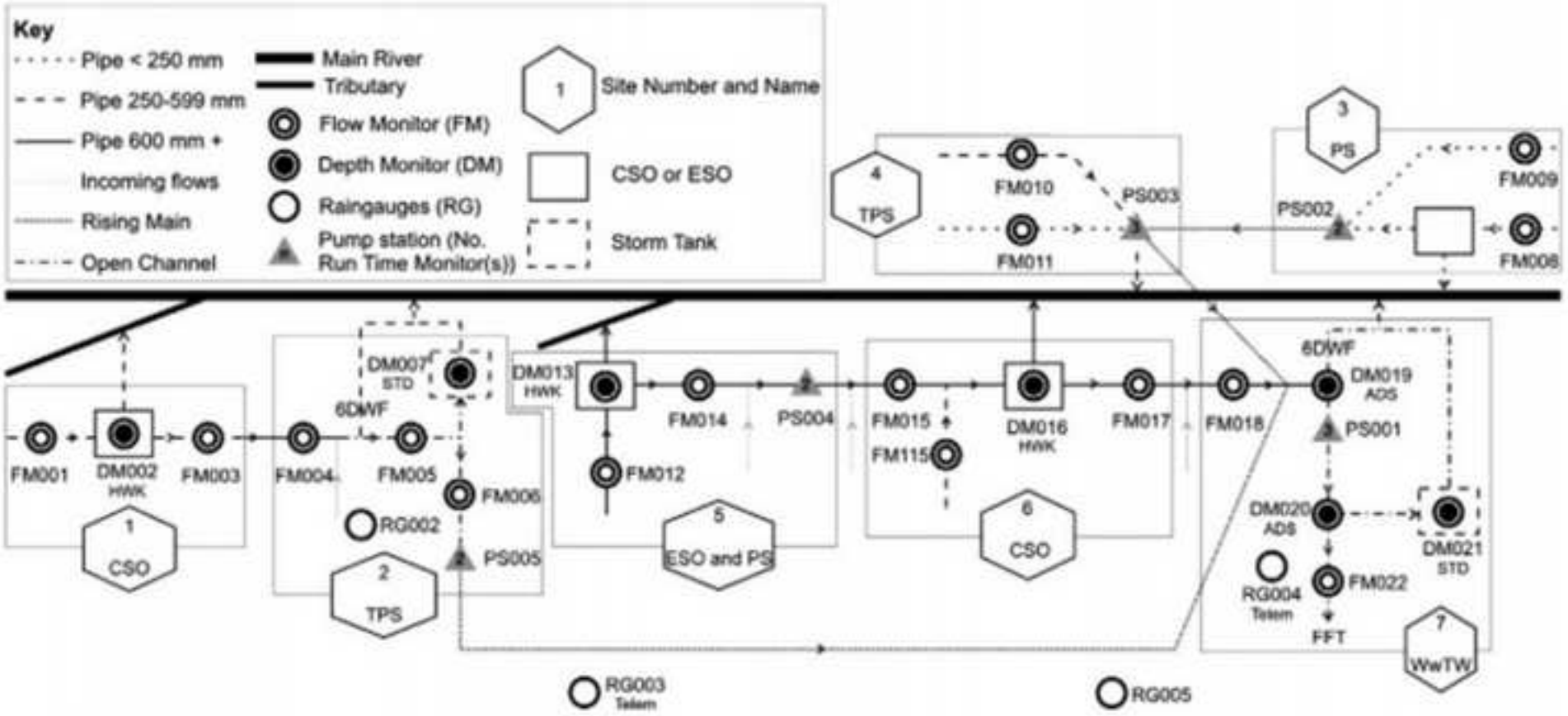

Figure 3

Click here to download high resolution image

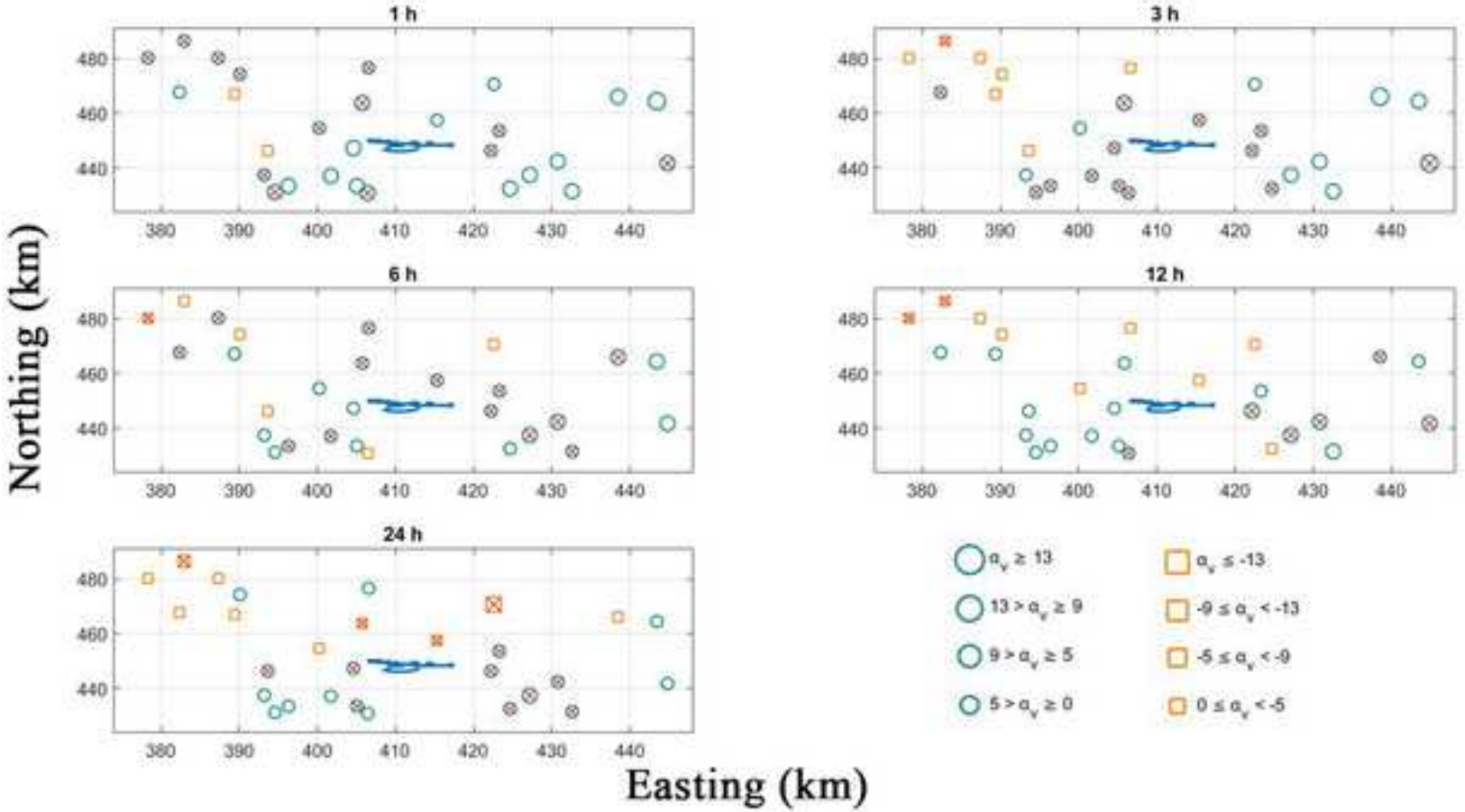

Figure 4

Click here to download high resolution image

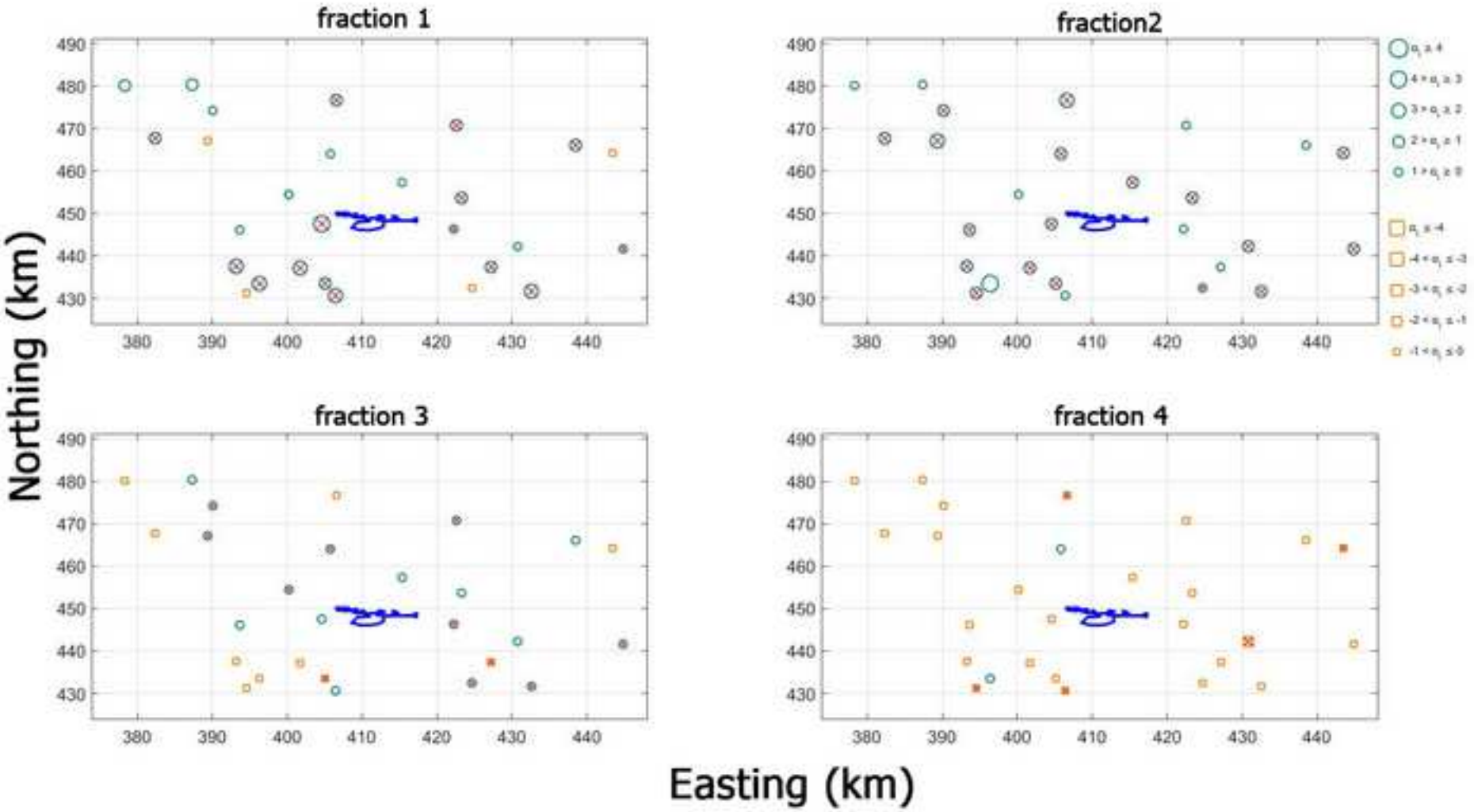

Figure 5

Click here to download high resolution image

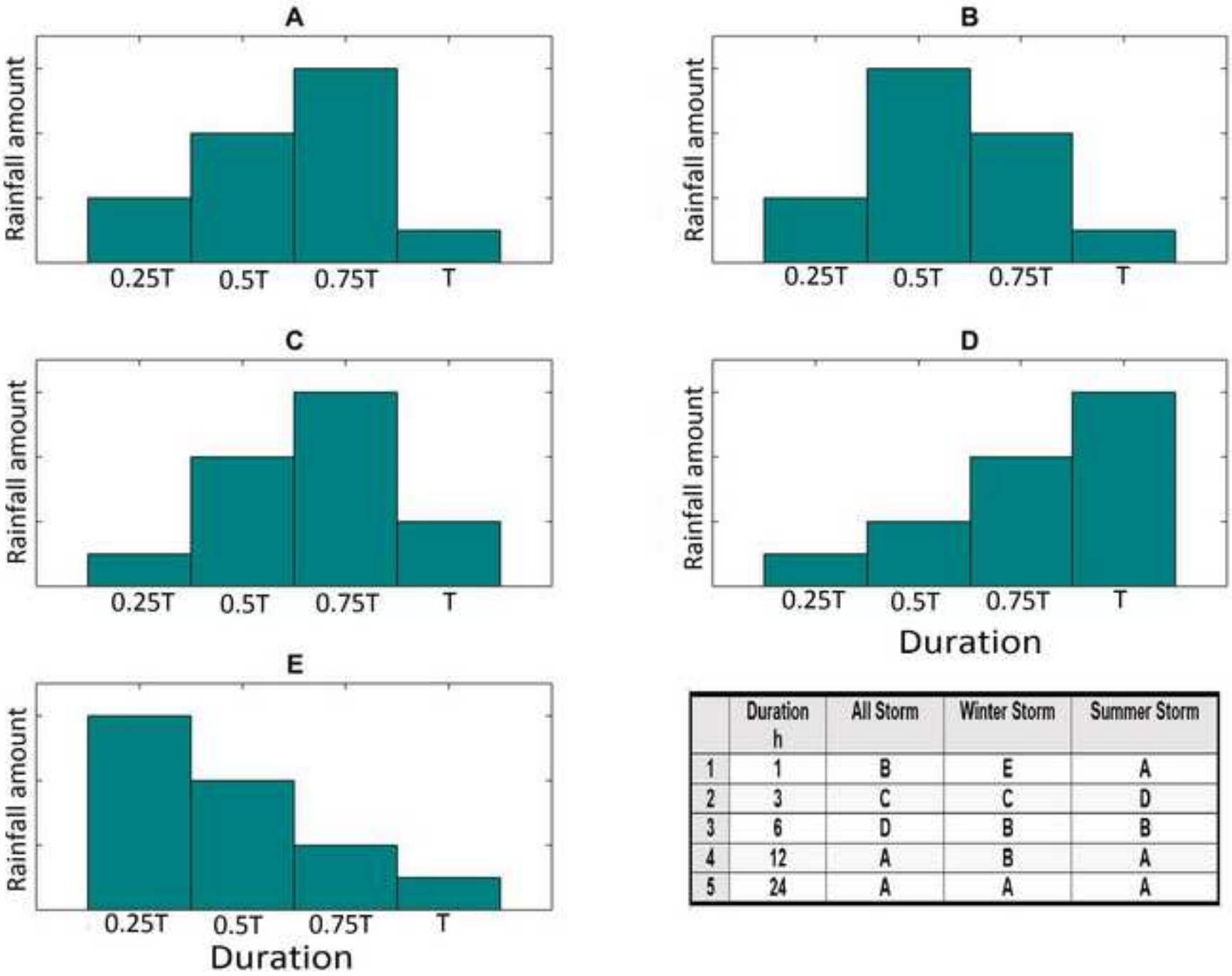

	Duration h	All Storm	Winter Storm	Summer Storm
1	1	B	E	A
2	3	C	C	D
3	6	D	B	B
4	12	A	B	A
5	24	A	A	A

Figure 6

Click here to download high resolution image

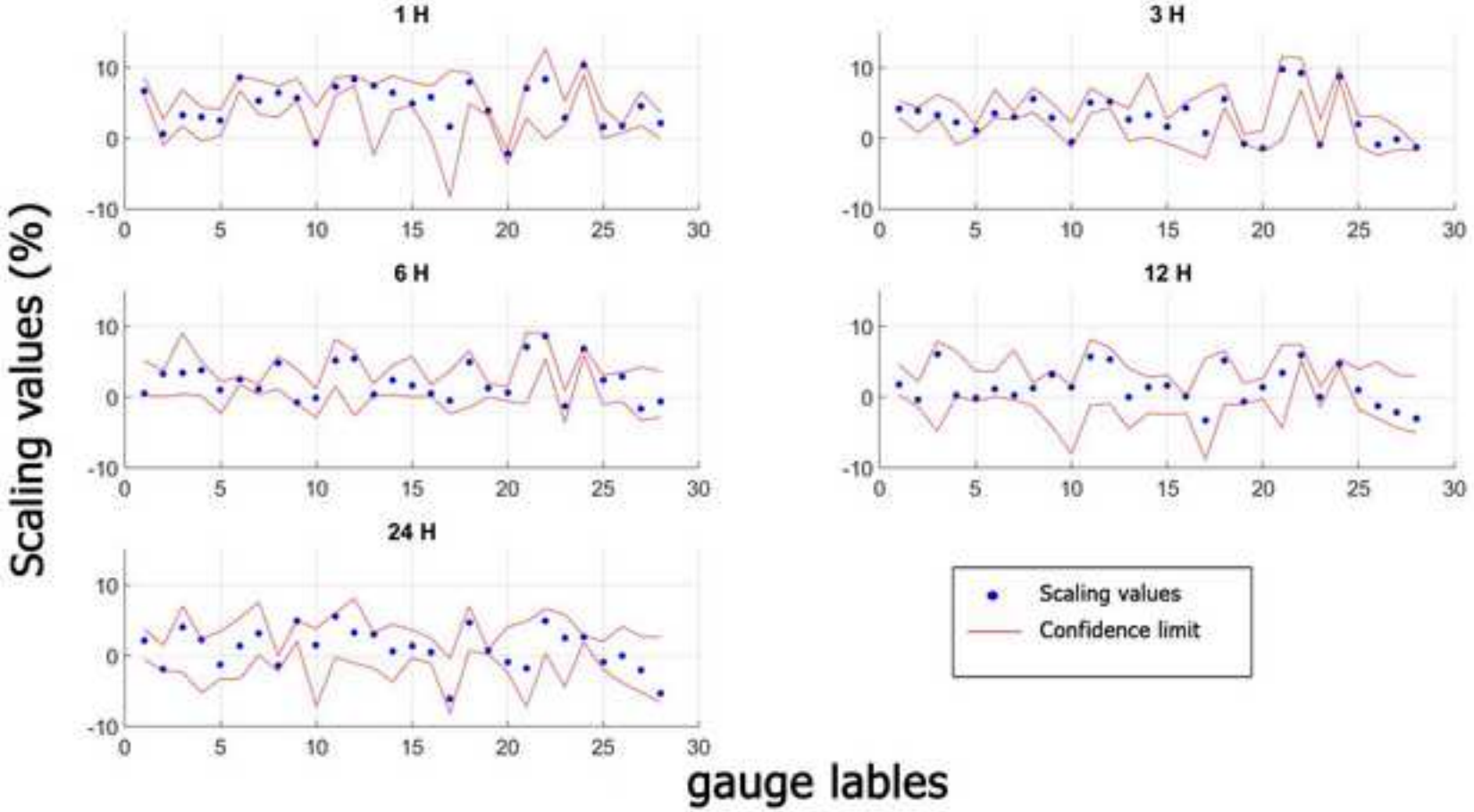

Figure 7

Click here to download high resolution image

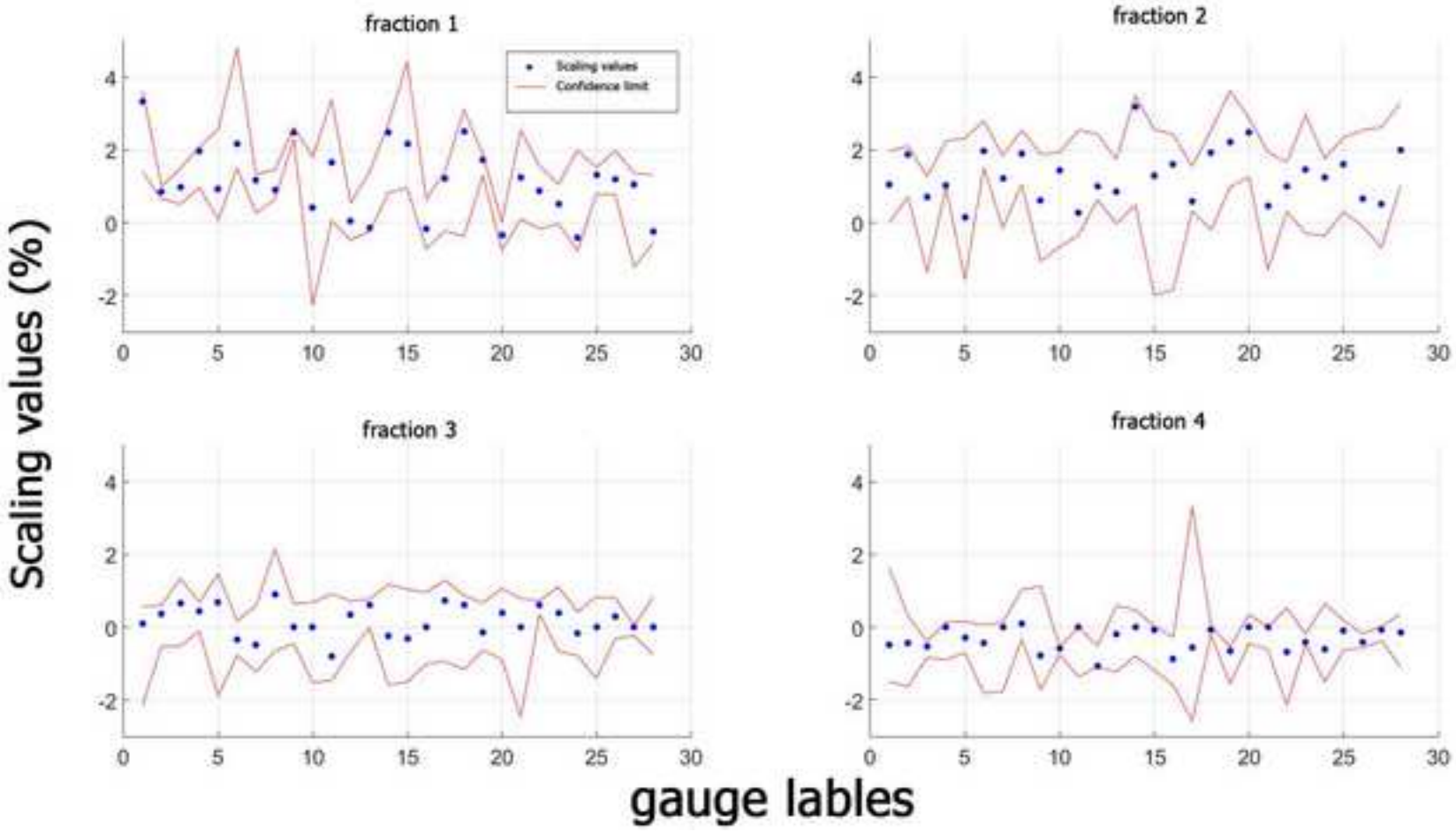

Figure 8

Click here to download high resolution image

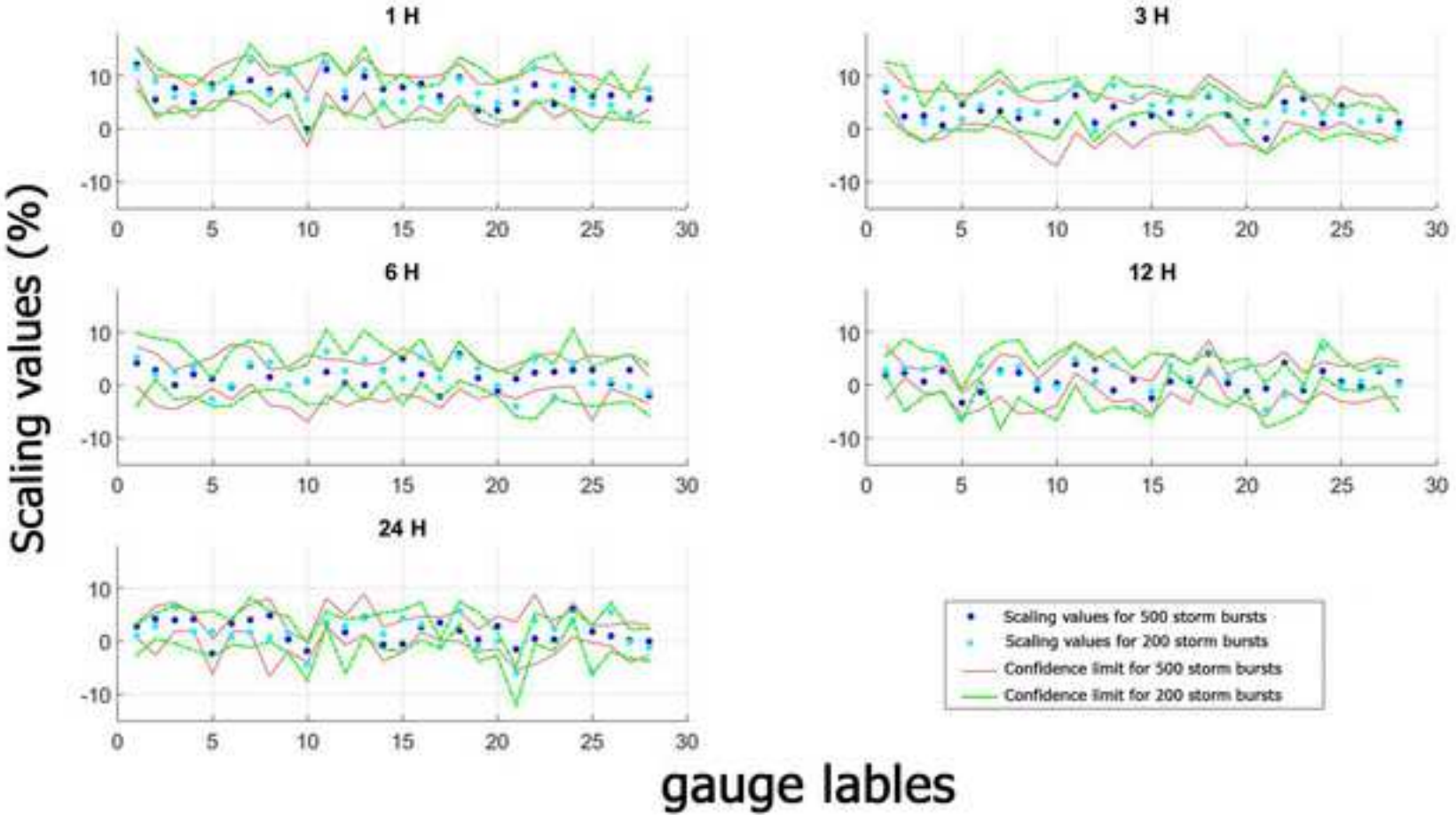

Figure 9

Click here to download high resolution image

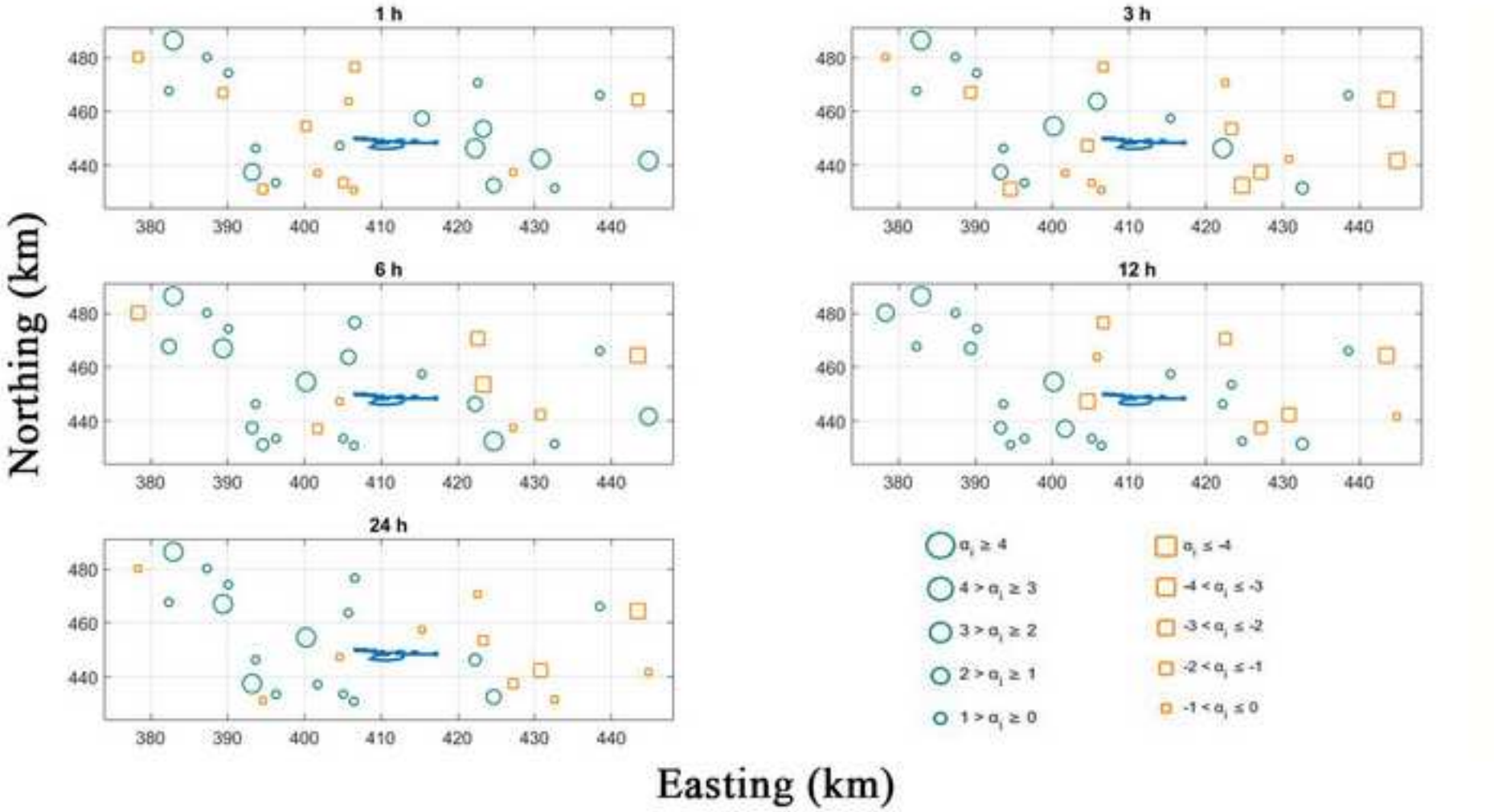

Figure S1

Click here to download high resolution image

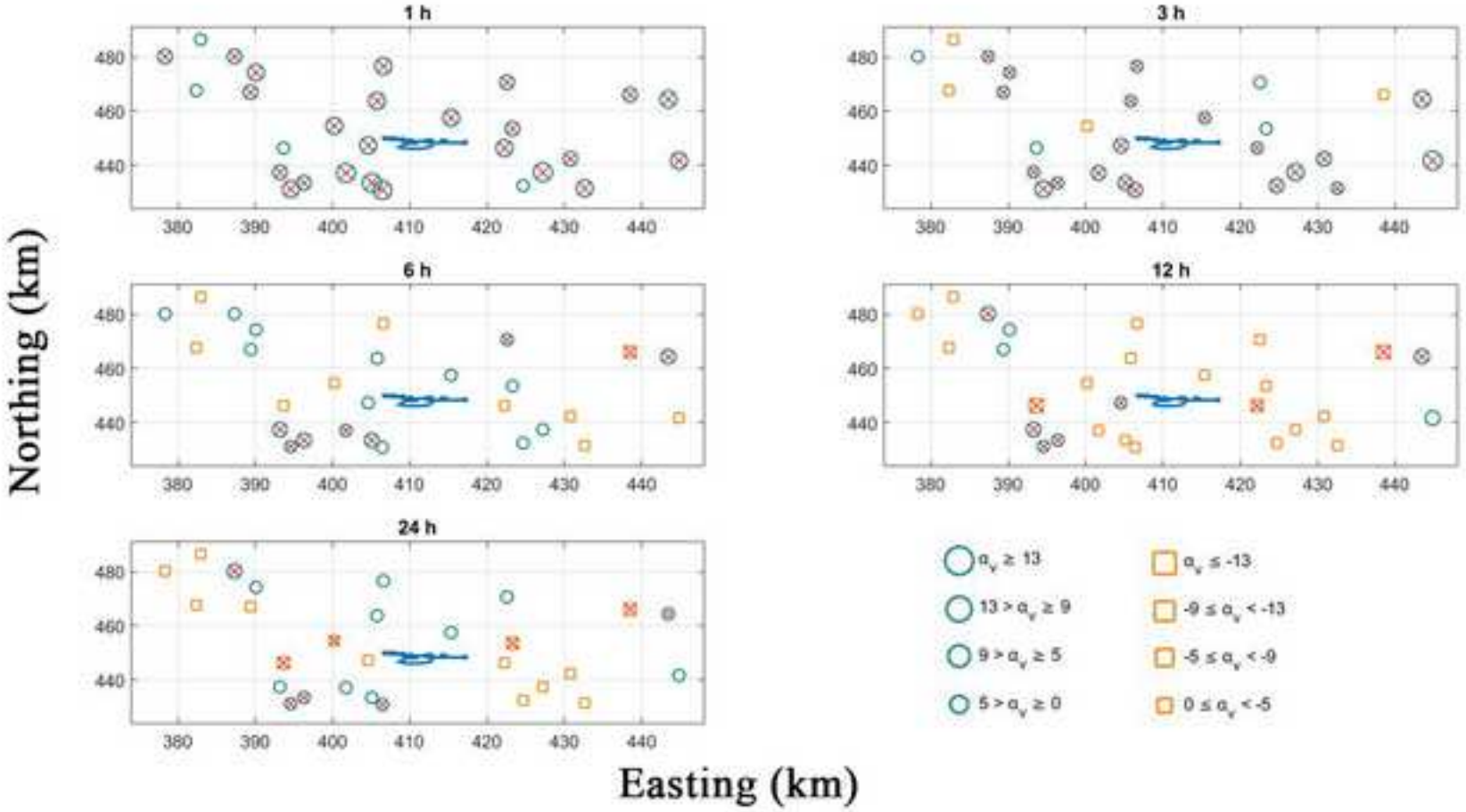

Figure S2

Click here to download high resolution image

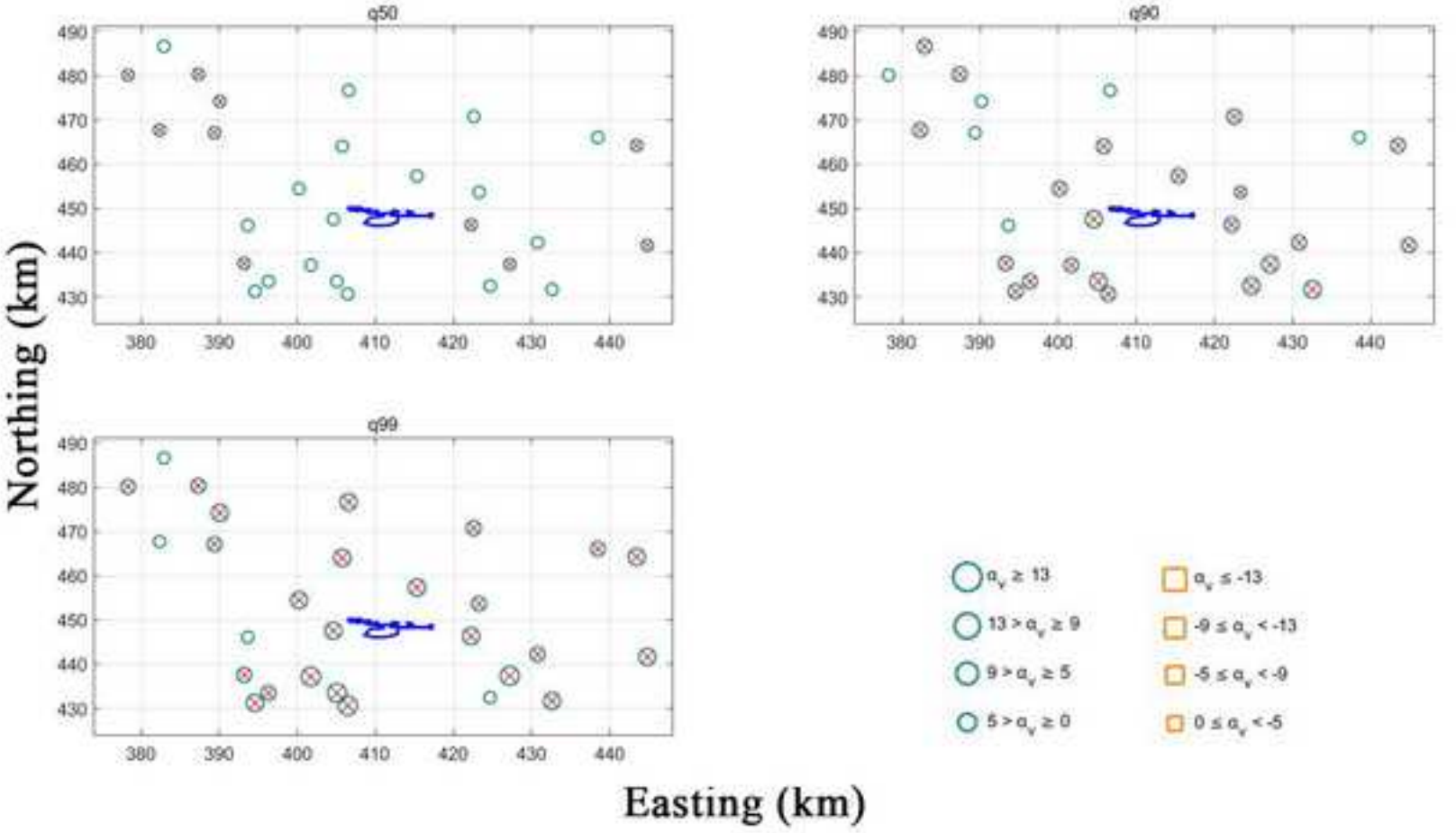

Figure S3

Click here to download high resolution image

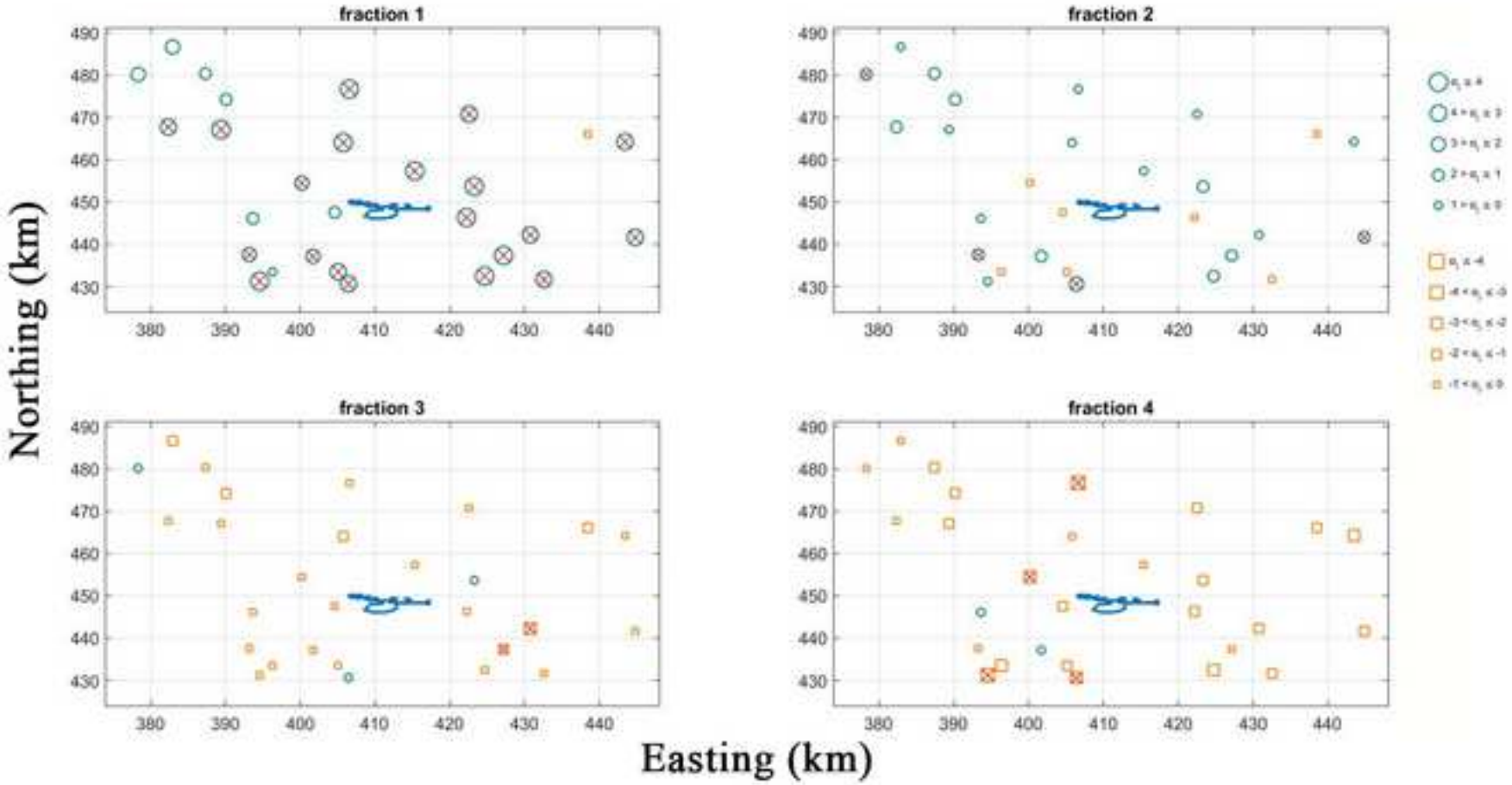

Figure S4

Click here to download high resolution image

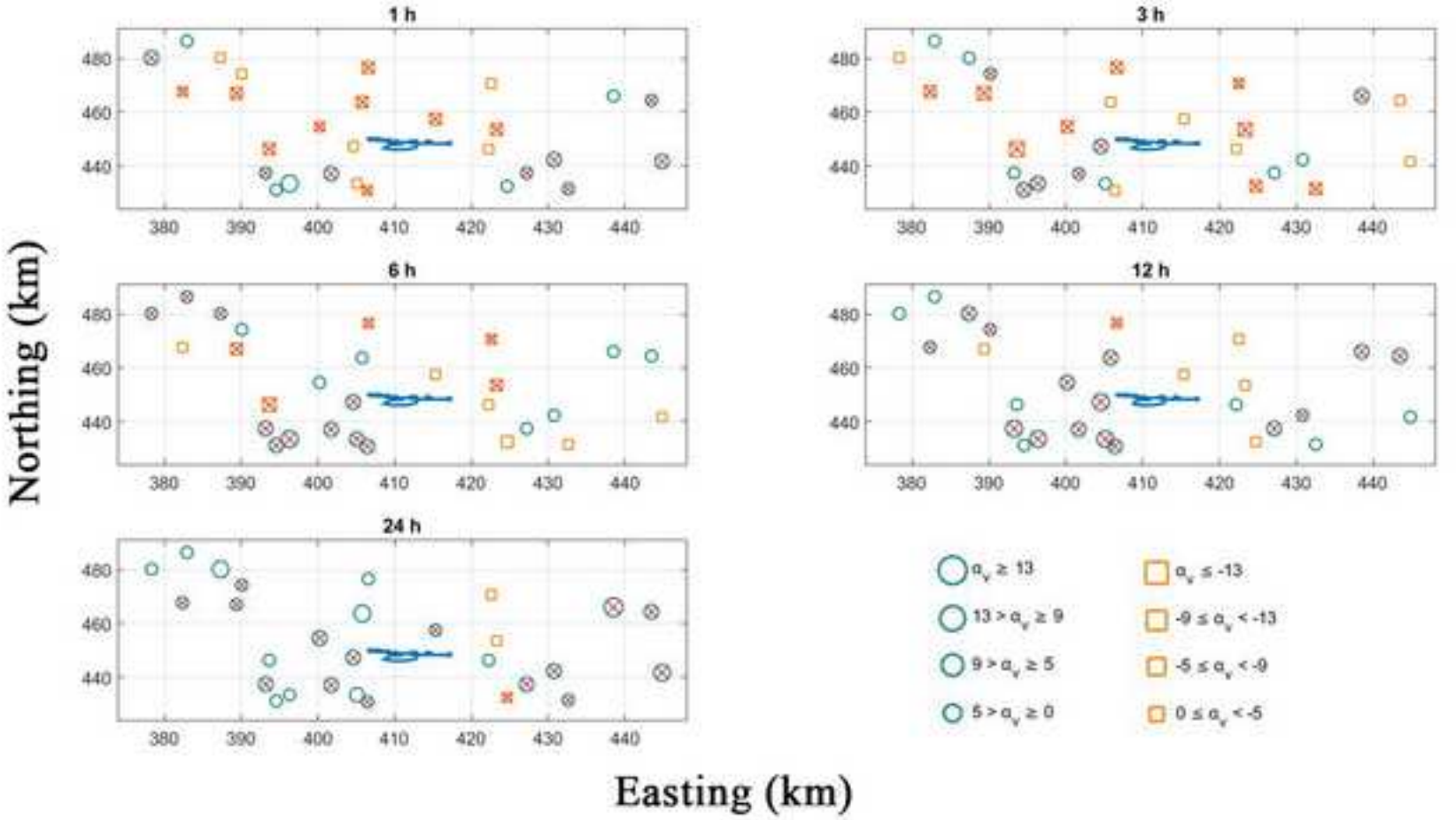

Figure S5

Click here to download high resolution image

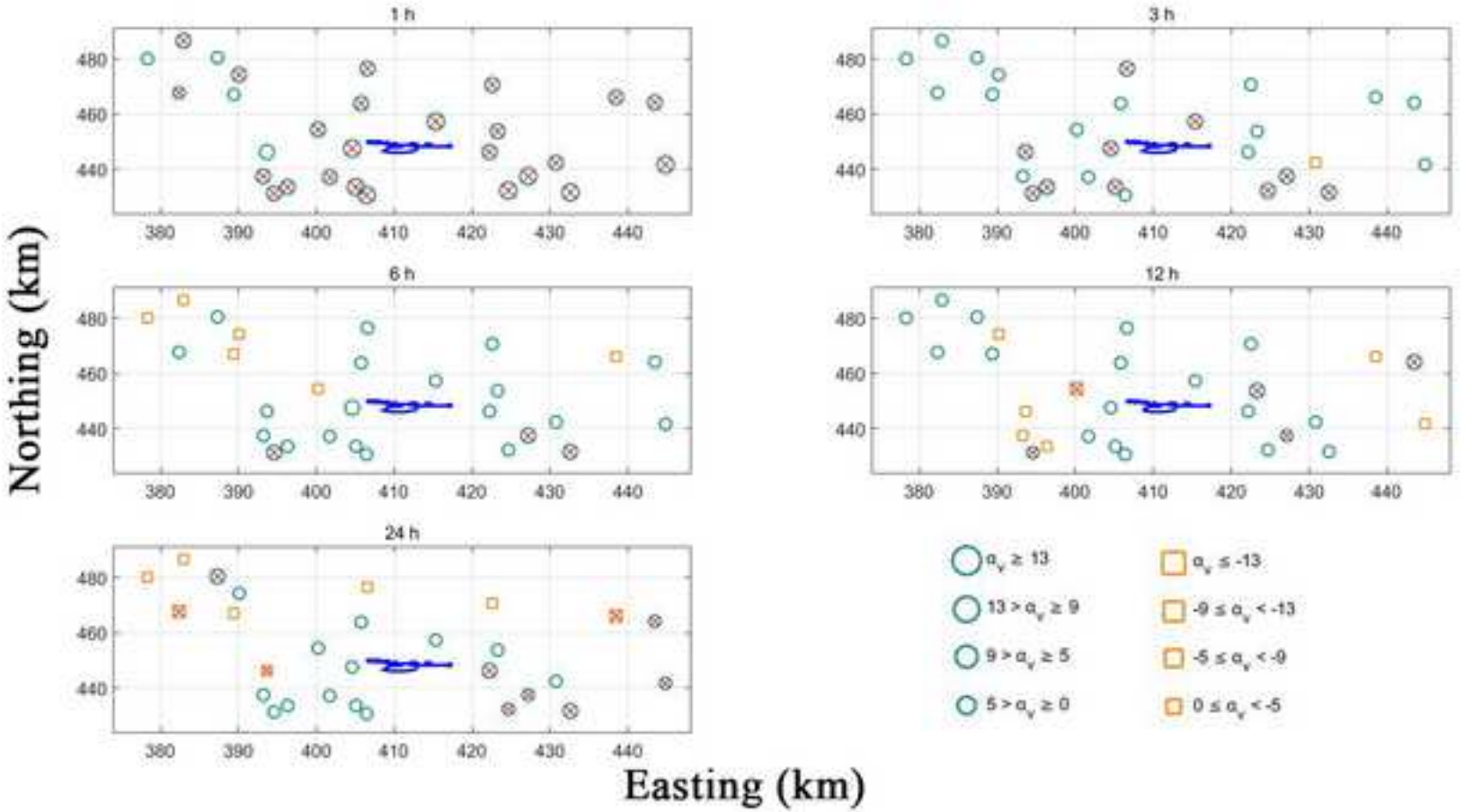

Figure S6

Click here to download high resolution image

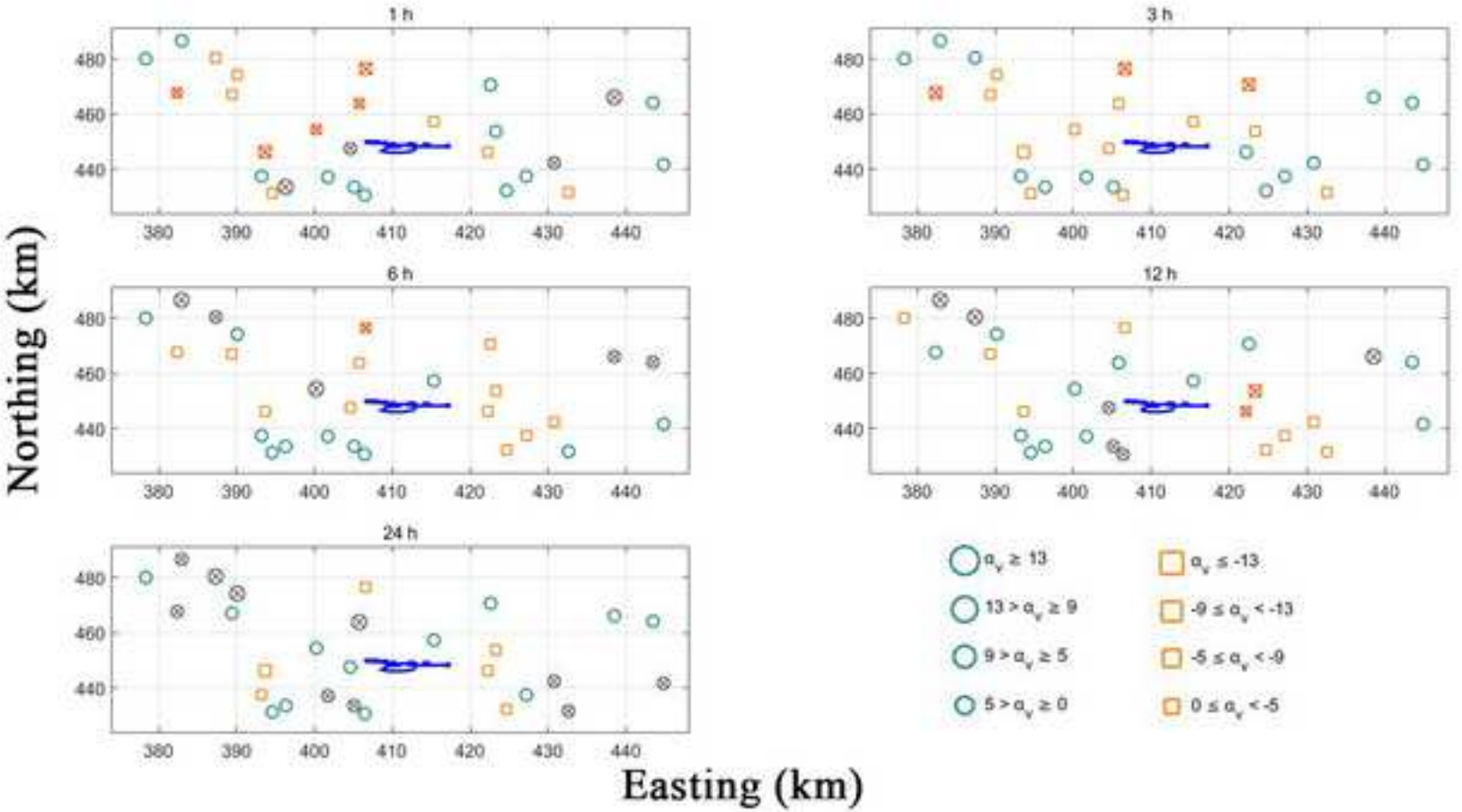

Figure S7

Click here to download high resolution image

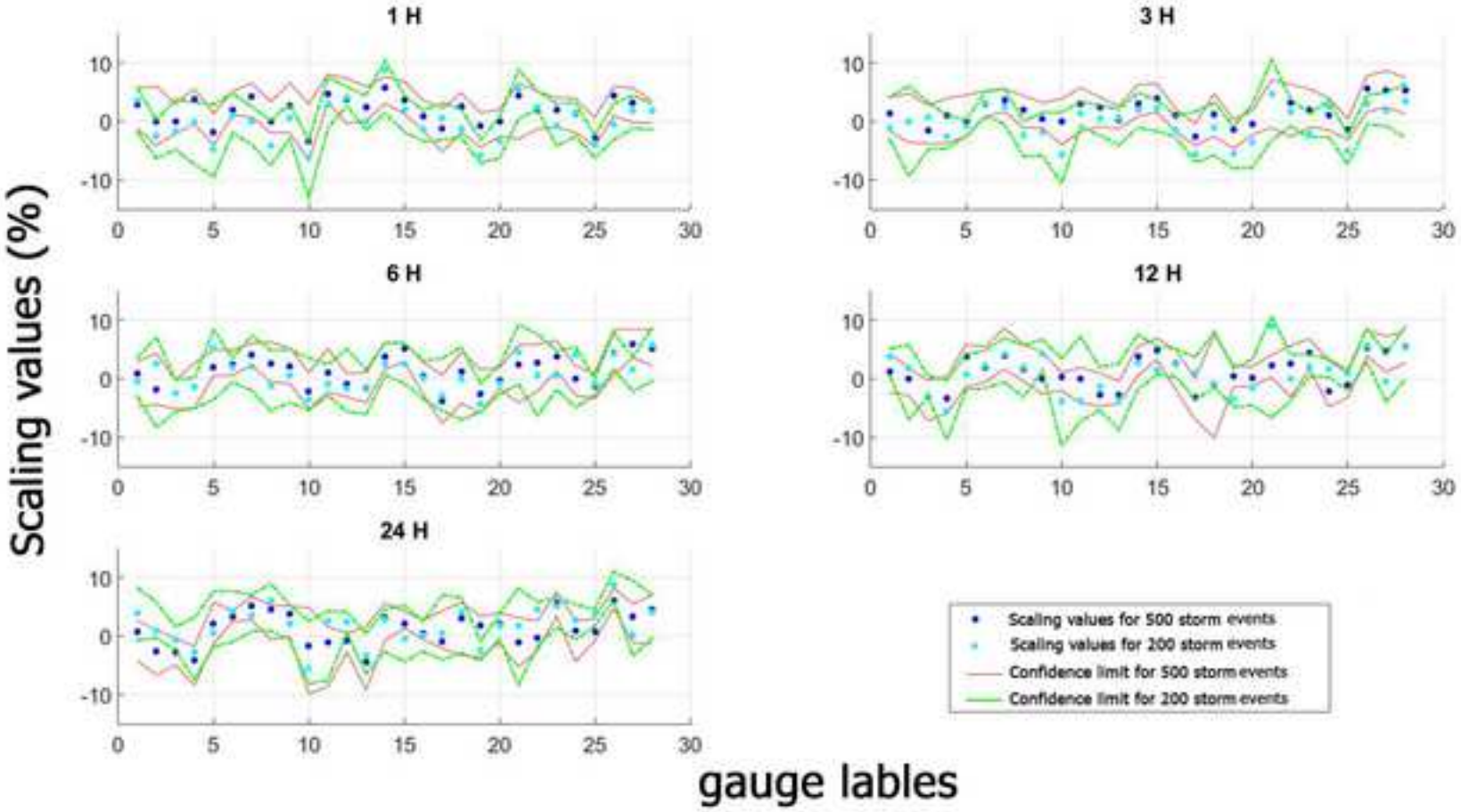

Figure S8

Click here to download high resolution image

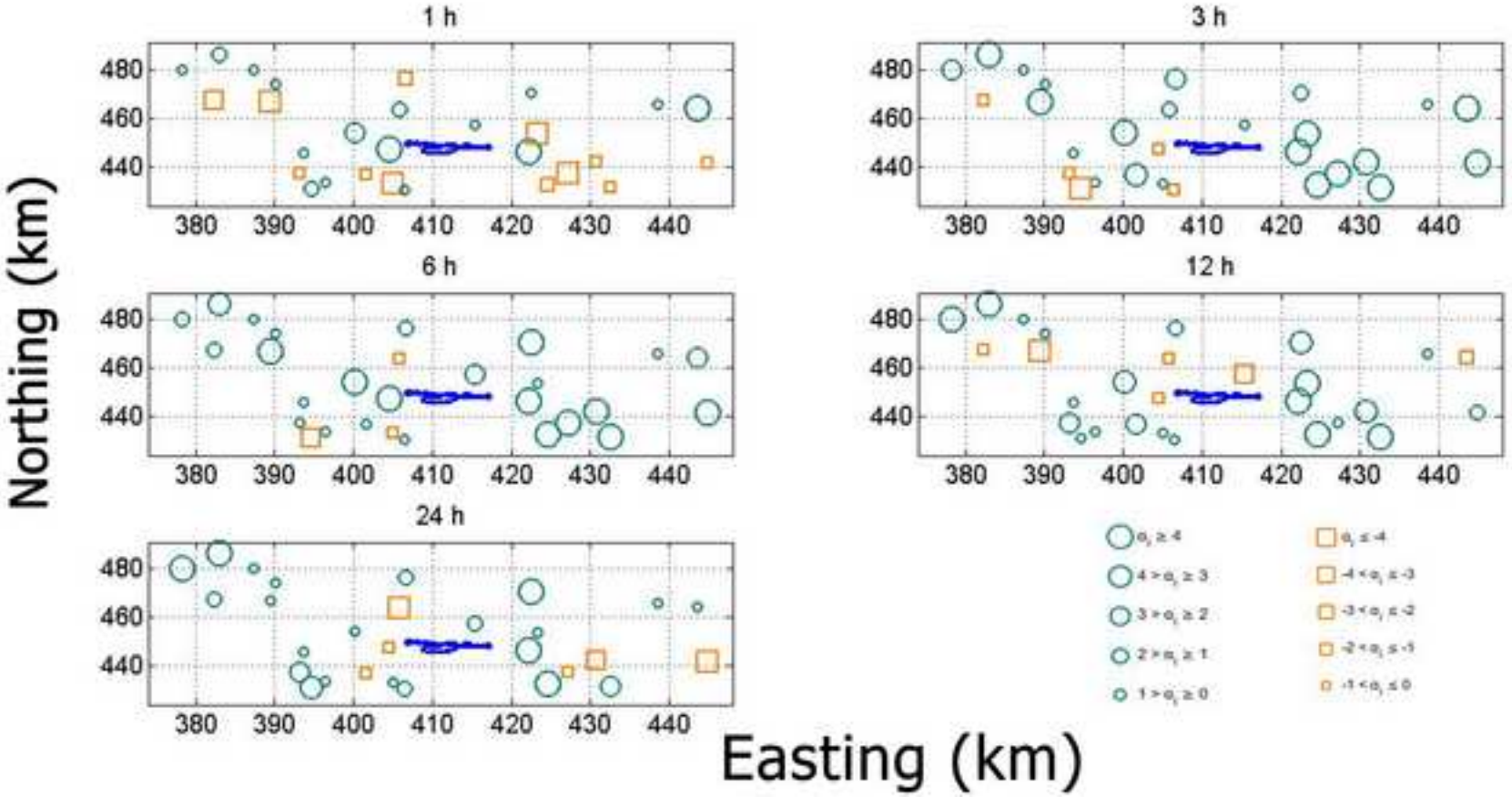

Figure S9

Click here to download high resolution image

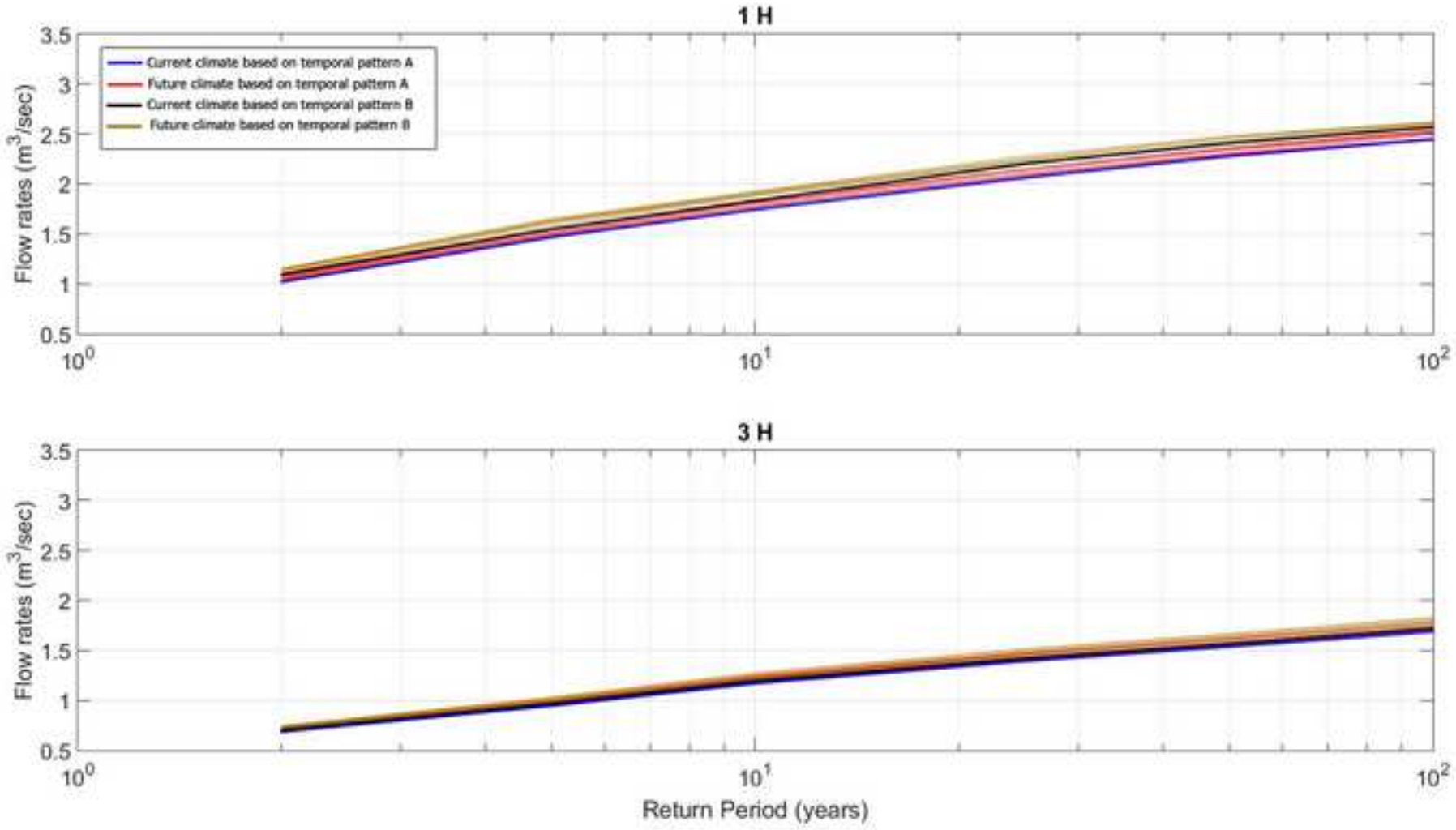

Figure S10

Click here to download high resolution image

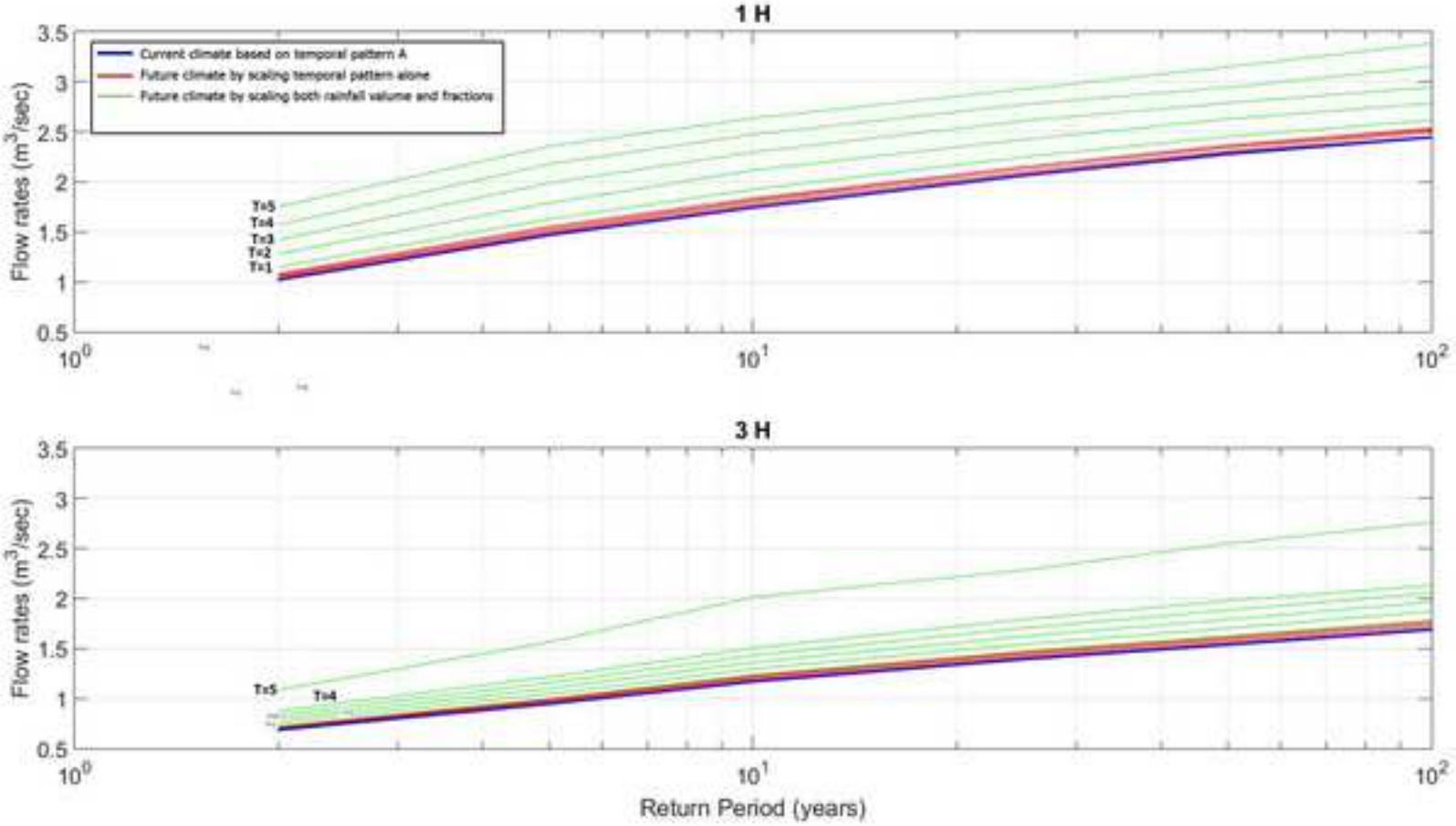

Figure S11

Click here to download high resolution image

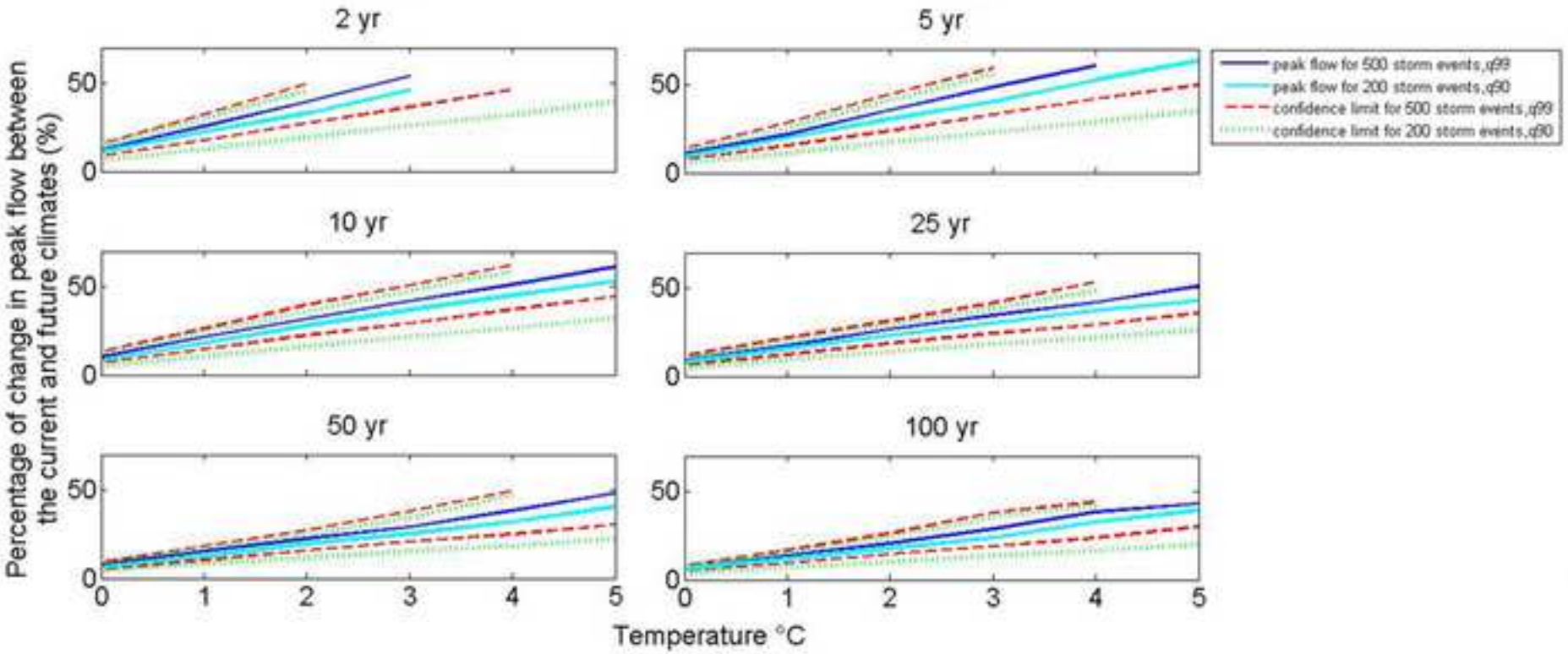

Figure S12

Click here to download high resolution image